Specialty Wood Products Research Partnership

UNIVERSITY OF CANTERBURY
Te Whare Wānanga o Waitaha
CHRISTCHURCH NEW ZEALAND

Theme: Specialty Wood Products (SWP)

PROJECT REPORT

Project No. SWP-T169

Experimental Studies on Single and Coupled Douglas-fir CLT Shear Walls with High-Capacity Connections

Authors:

Minghao Li
Ben Moerman

Research Provider: UC

Date: 29 May 2023

Contents

EXECUTIVE SUMMARY

As an engineered timber product, cross-laminated timber (CLT) is currently gaining popularity in New Zealand and globally. This two-year project aims to develop high-capacity Douglas-fir CLT shear wall structures that are suitable for multi-storey mass timber buildings constructed in high seismic countries like New Zealand. A total of seven Douglas-fir CLT shear wall specimens were cyclically tested to evaluate their strength, stiffness, ductility and hysteretic behaviour. The wall specimens consisted of six single cantilever walls and one coupled wall with steel link beams. The results showed all the wall specimens exhibited significantly higher strength and stiffness than conventional CLT shear walls in literature. In particular, the coupled wall with steel link beams and mixed angle screwed hold-downs achieved high capacity and high ductility. In comparison to similar cantilever CLT shear walls, the coupled wall exhibited 45% higher peak strength, dissipated 50% more energy, and experienced less degradation of energy dissipation. The coupled wall was also repaired and re-tested. The repaired wall showed comparable performance to the original wall, indicating the feasibility of the repair strategy developed by this study.

1. INTRODUCTION

Cross-laminated timber (CLT) consists of orthogonal layers of timber boards which are glued together to create solid panels with timber fibres oriented in both orthogonal directions. The crosswise layup improves dimensional stability and homogeneity of the mass timber panels. CLT can be used horizontally as floor or roof plates to resist gravity loads and vertically as walls to resist gravity, wind, and seismic loads. CLT panels are commonly available in a range of thicknesses up to 300mm. Compared to light-timber frame (LTF) walls with plywood or oriented strand board (OSB) sheathing, CLT panels have significantly greater in-plane strength and stiffness. However, most conventional CLT walls are constructed with connections that resemble those used in LTF construction (i.e., light gauge metal brackets with ring shank nails or screws). By using stronger and stiffer connections, the strength and stiffness of the CLT shear wall system can be increased.

Conventional CLT shear walls are a feasible lateral load resisting systems (LLRS) in seismic regions and are currently recognized by various building codes such as National Building Code of Canada (NBCC 2020) [1] and the American Design Standard ASCE 7-22 [2], with restrictions and design guidance in the Special Design Provisions for Wind and Seismic (SDPWS) [3]. Both codes require walls to have a height-to-length aspect ratio between 2:1 to 4:1 and prefer energy dissipation by a rocking mechanism, rather than sliding or a combination of the two modes. Recently, Pei et al. [4] and Izzi et al. [5] completed state-of-the-art reviews of CLT shear wall research for seismic LLRSs. Based on previously completed CLT shear wall experiments and analytical work, both studies identified the deformation of a CLT wall as being primarily governed by rigid body movement (sliding and/or rotation) and the lateral strength being controlled by its base connections. Previous cyclic and dynamic experiments have included single CLT walls, multi-panel assemblies, and whole buildings intended for platform-type construction. However, the focus of this study is on single CLT shear walls for balloon-type construction.

Single, or cantilever, CLT shear walls can achieve a ductile failure mechanism through well-detailed base connections. Conventional base connections consist of cold-formed steel brackets (approximate thickness of 3mm or less) with groups of small diameter (d<6mm) nails or screws fastening the bracket to the CLT surface, as described in the previously mentioned state-of-the-art reviews [4,5]. Typically, hold-down (HD) connectors are installed at the ends of walls to resist the base moment and angle brackets are provided along the to resist the lateral shear force. To investigate the lateral capacity of conventional CLT shear walls, key results from several 1-storey, cyclic tests of single walls are summarized in *Table 1*. A brief description of the strongest wall specimen in each experimental programme is presented with its peak strength and initial stiffness (where available). Two additional parameters were determined for each wall. First, a strength

utilization factor (λ) was calculated, according to Equation *(1)*, that describes the ratio of peak load to nominal panel strength (i.e. partial safety factor of γ=1 according to Eurocode 5 [6]). The shear and bending stresses occurring at peak load (F_{max}) were compared to the panel's nominal gross shear and bending strengths, respectively (first and second terms in Equation *(1)*, respectively). Second, a peak quasi-uplift force demand (T') of the HD connection was calculated with an approximate method from Casagrande et al. [7], shown in Equation *(2)*. While more rigorous methods have been proposed to determine the uplift demand of a HD (Lukacs et al. [8]), an approximate force demand was used here for general comparison and discussion.

$$\lambda = MAX\left(\frac{3F_{max}}{2A_g k_{mod} f_{v,k}}, \frac{6F_{max}H}{t_{pr}L^2 k_{mod} f_{b,k}}\right) \quad (1)$$

$$T' = \frac{F_{max}H}{0.9L} \quad (2)$$

where F_{max} is the absolute peak experimental force
A_g is the gross cross section area
H is the height of the applied load
t_{pr} is the CLT thickness oriented vertically in the primary layers
L is the wall length
k_{mod} is the loading rate modification factor from the relevant timber design standard
$f_{v,k}$ is the characteristic shear strength for the given CLT grade, and
$f_{b,k}$ is the characteristic bending strength for the given CLT grade

Table 1: Summary of 1-storey, cyclic CLT wall tests in literature

Research source (specimen ID)	**CLT wall dimensions T x L x H (mm)**	**Aspect Ratio, H/L**	**Hold-down connection**	**CLT Grade**	**Peak lateral force, F_{max} (kN)**	**Strength utilization, λ**	**Quasi-uplift force demand, T' (kN)**
Dujic et al. [9] (W14c_C_V1/1)	94 x 3200 x 2720 (31/31/31)	0.9	Light steel angle w/ 10-Ø4x40 ring shank nails	C24[a]	70	9%	66
Lauriola et al. [10] (A_1)	85 x 2950 x 2950 (17/17/17/17/17)	1.0	Custom plate w/ 29-Ø4x60 ring shank nails	C24[a]	141	21%	157
Okabe et al. [11] (1P)	90 x 1000 x 3000 (30/30/30)	3.0	Light steel w/ 20-Ø3.3x65 ring shank nails	Sugi[b]	45	-	150
Popovski and Karacabeyli [12] (CB-SN-14)	94 x 3450 x 2300 (31/31/31)	0.7	Simpson Strong-Tie 90x105x105mm angle w/ 10-16d spiral nails[f]	C24[a]	191	30%	141
Popovski and Karacabeyli [12] (CA-SN-20)	94 x 2300 x 2300 (31/31/31)	1.0	BMF 90x48x116mm angle w/ 18-16d spiral nails[f]	C24[a]	152	24%	169
Hummel et al. [13]	105 x 2500 x 2500	1.0	Simpson Strong-tie HTT22	C24[c]	126	18%	140

(W-CLT-2.3)	(21/21/21/21/21)		w/ 17-Ø4x60 ring shank nails				
Flatscher et al. [14] (E)	112 x 2500 x 2500 (33/33/33)	1.0	Simpson Strong-tie HTT22 w/ 15-Ø4x60 ring shank nails	C24[a]	76	9%	84
Gavric et al. [15] (I.4)	85 x 2950 x 2950 (17/17/17/17/17)	1.0	Simpson Strong-tie HTT22 12-Ø4x60 ring shank nails	C24[a]	107	16%	119
Pozza et al. [16] (1B)	85 x 2950 x 2950 (17/17/17/17/17)	1.0	Simpson Strong-tie HTT22 12-Ø4x60 ring shank nails	C24[a]	105	16%	116
Amini [17] (25)	169 x 1220 x 2440 (34/34/34/34/34)	2.0	2-Ø¾" rods	E1[d]	130	39%	288
Li et al. [18] (S2)	105 x 1200 x 2000 (35/35/35)	1.7	Custom bracket w/ 8-Ø5x80 self-tapping screws	V2[e]	35	31%	65
Amini et al. [19]	90 x 610 x 2240 (not reported)	3.7	Simpson Strong-Tie HDU8 and Ø16mm threaded rod w/ 20-Ø6x64mm SDS screws	C24[c]	25	57%	102

As shown in *Table 1*, most of the tested 1-storey CLT walls had a thickness less than 125mm and used cold-formed steel plate HDs with ring shank nails. A maximum strength utilization of 57% was reported by Amini et al. [19], however, ten of the twelve tests in *Table 1* had a strength utilization of 31% or less. Capacity design requires the nominal strength of a brittle element (e.g. CLT wall panel) to exceed the overstrength of the ductile element (e.g. slender HD fasteners) to prevent brittle failure modes. Therefore, the most efficient theoretical design would use a CLT wall panel with a strength utilization ratio of 100% when subjected to the overstrength demand of the HD connection. However, it is apparent that commonly available HD connectors are not typically able to reach strength utilization factors approaching 100% for 1-storey walls with typical dimensions of approximately 100mm in thickness and 2 to 3m in length. To achieve greater strength utilization ratios, particularly with thicker CLT panels, it may become impractical to use a large number of small fasteners due to the constraints of connection areas and low capacity of individual small fasteners. Therefore, high-capacity hold-down connections with larger fasteners such as dowels, bolts, or self-tapping screws (d>6mm) can be more practical.

A new type of high-capacity HD with Ø12mm mixed angle self-tapping screws in a 5-ply, 175mm-thick Douglas-fir CLT was cyclically tested by Wright et al. [20]. The combination of inclined (45°) and normal (90°) screws created a connection with relatively high initial stiffness to limit interstorey drifts during service-level seismic or wind events while also providing a ductile failure mode to dissipate energy in severe earthquakes. The inclined screws were only partially threaded to

promote a ductile withdrawal failure rather than a sudden, brittle tensile fracture of the screw shank. The largest connection specimens had peak strengths exceeding 600kN and initial stiffnesses greater than 200kN/mm. Wright et al. [20] also compared the results to the dowel connections tested by Ottenhaus et al. [21] and found that the mixed angle screw HD showed greater initial stiffness (although the mean specimen strength was approximately 30% less), comparable displacement capacity, greater ductility, but lower total energy dissipation due to a more severely pinched hysteresis.

The limited lateral capacity of commercial HDs and angle brackets in conventional CLT shear walls limits their application in mid-rise or high-rise CLT buildings subjected to significant wind or earthquake loads. Presently, high-capacity HDs using dowels and mixed angle screws have only been tested at the component level – not as part of laterally loaded wall experiments. This study presents an experimental programme to evaluate the cyclic behaviour of a total of seven large scale high-capacity CLT shear walls with custom HD and shear key elements. The purpose of this study is to provide insights and experimental results to inform the design of more efficient, high-capacity CLT shear walls with well-detailed HD solutions suitable for mid-rise or taller CLT buildings in New Zealand and other seismic regions.

2. SINGLE WALL TESTS

2.1 Test matrix

Six CLT wall specimens were cyclically tested, as described in *Table 2*, in the Structural Engineering Laboratory at the University of Canterbury. These specimens included three different height-to-length aspect ratios (0.52, 1.3, and 3.3) and two HD types (bolted and screwed). *Figure 1* shows the base connection locations and height of loading points for the three different wall geometries. Each wall specimen used a 5-ply CLT panel (45/35/45/35/45mm) fabricated from New Zealand Douglas Fir boards. The primary layers used 45x190 SG8 boards and the cross layers used 35x140 SG6 boards (timber grades defined in the New Zealand Timber Structures Standard NZS3603 [22]). The mean density was 484 kg/m^3 (COV 0.12) and the mean moisture content was 11.4% (COV 0.072).

Table 2: Test matrix.

Test ID	**Aspect Ratio, H/L**	**CLT Wall Dimensions L x H (mm)**	**Hold-down Connection**	**D_{ref} for CUREE protocol (mm) / (drift ratio %)**
B_0.52	0.5	5000 x 2600	4 - Ø16mm bolts	30 / 1.2%
S_0.52	0.5	5000 x 2600	Mixed angle screws 4 - Ø12X260 PT[a] CSK[b] @ 45° 6 - Ø12X180 PT CSK @ 90° Each side	30 / 1.2%
B_1.3	1.3	2000 x 2600	4 - Ø20mm bolts	65 / 2.5%
S_1.3	1.3	2000 x 2600	Mixed angle screws 8 - Ø12X260 PT CSK @ 45° 12 - Ø12X180 PT CSK @ 90° Each side	65 / 2.5%
B_3.3	3.3	2000 x 6600	4 - Ø20mm bolts	198 / 3.0%
S_3.3	3.3	2000 x 6600	Mixed angle screws 8 - Ø12X260 PT CSK @ 45° 12 - Ø12X180 PT CSK @ 90° Each side	198 / 3.0%

a) PT = Partially threaded
b) CSK = Countersunk head

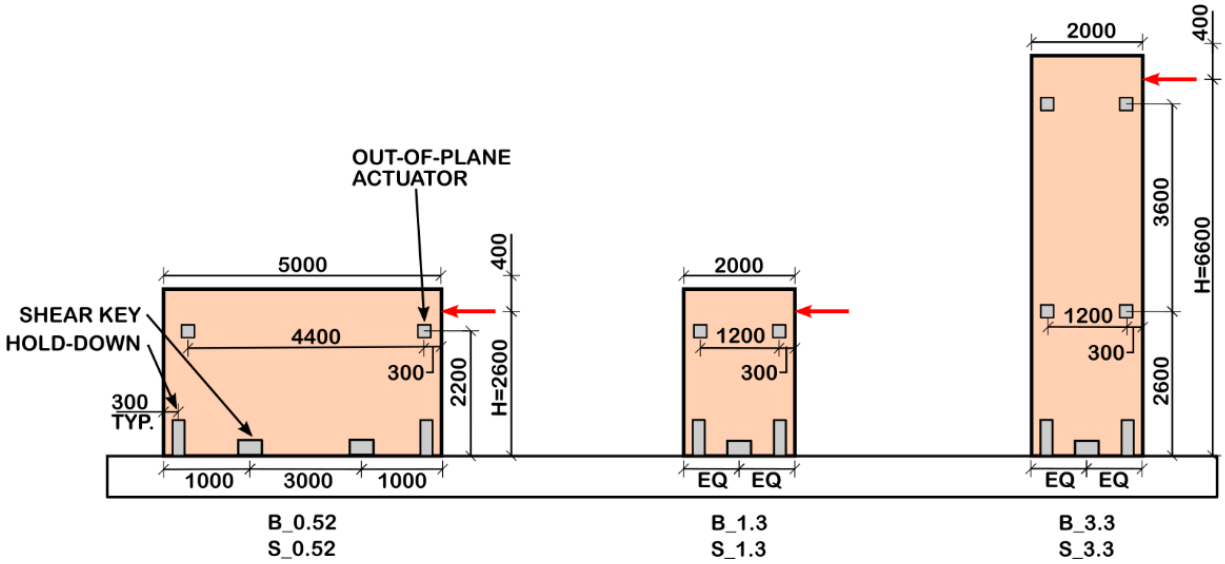

Figure 1: General arrangement of tested CLT wall specimens.

2.2 Setup and loading protocol

A representative test setup is shown in *Figure 2*. A 1000kN hydraulic actuator applied in-plane loading through a spherical bearing connected to a steel clamp with 8-M30 threaded rods near the top of the wall. The control displacement was measured by a string potentiometer adjacent to the primary actuator. Additional actuators were connected to the wall by pinned connections with spherical bearings to provide points of out-of-plane translational restraint (in the y-direction of *Figure 2*). No out-of-plane displacement demands were imposed on the specimens. The bottom edge of the wall was connected by HDs at each end and an internal shear key which were bolted to the steel base fittings. The steel bases were bolted to the concrete strong floor by M36 threaded rods at a 400mm spacing in each direction. Aside from the self-weight of the actuators and clamp attached to the walls (weight of 14kN and 18kN for walls loaded at 2.6m and 6.6m, respectively), no additional vertical load was applied to the specimens.

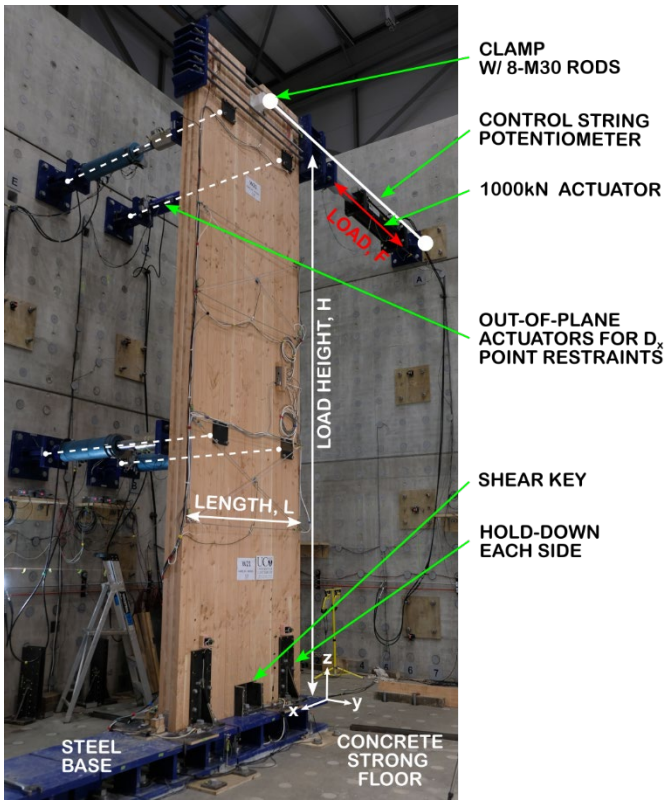

Figure 2: Test setup for cyclic CLT wall testing.

Each specimen was subjected to the CUREE loading protocol [23], which applies a series of primary and trailing (80% of primary magnitude) cycles. An example of the protocol is shown in *Figure 3*. Reference displacements are used to define the CUREE protocol and were estimated based on nonlinear pushover analyses of each specimen and are listed in *Table 2*. The pushover models were created in SAP2000 using linear-elastic beam elements to represent the CLT panels and nonlinear links for the HD elements with approximate properties based on test data from similar component test results [20].

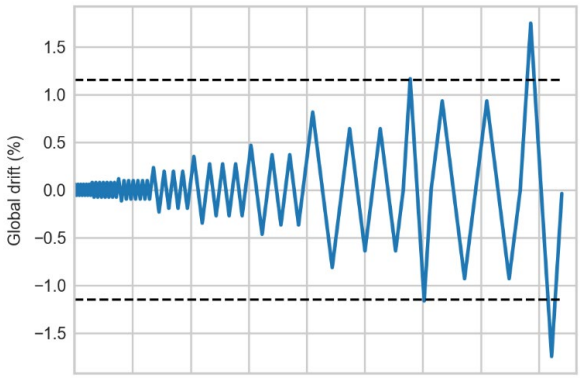

Figure 3: Example of the CUREE loading protocol for specimens B_0.52 and S_0.52 (D_{ref}=1.2% drift).

2.3 Base connection details

Typical bolted HDs used in three of the test specimens are shown in *Figure 4*a and *4b*. The bolts were made from round mild steel bar (specified f_y=300MPa) and the ends were threaded to receive a nut on each side. A typical 25mm-thick side plate was used to increase fixity at the ends of each bolt and increase the number of plastic hinges formed when yielding. The steel side plates were fabricated to use a maximum of 8 bolts but only 4 were used in each test.

Examples of the mixed angle screw HDs are shown in *Figure 4*c and *4d*. Each HD was installed symmetrically at each end of the wall with a combination of self-tapping screws installed at 45° and 90° angles. The perpendicular to grain spacing of the screws (a_2) was varied to prevent conflict between screws installed from each side of the wall.

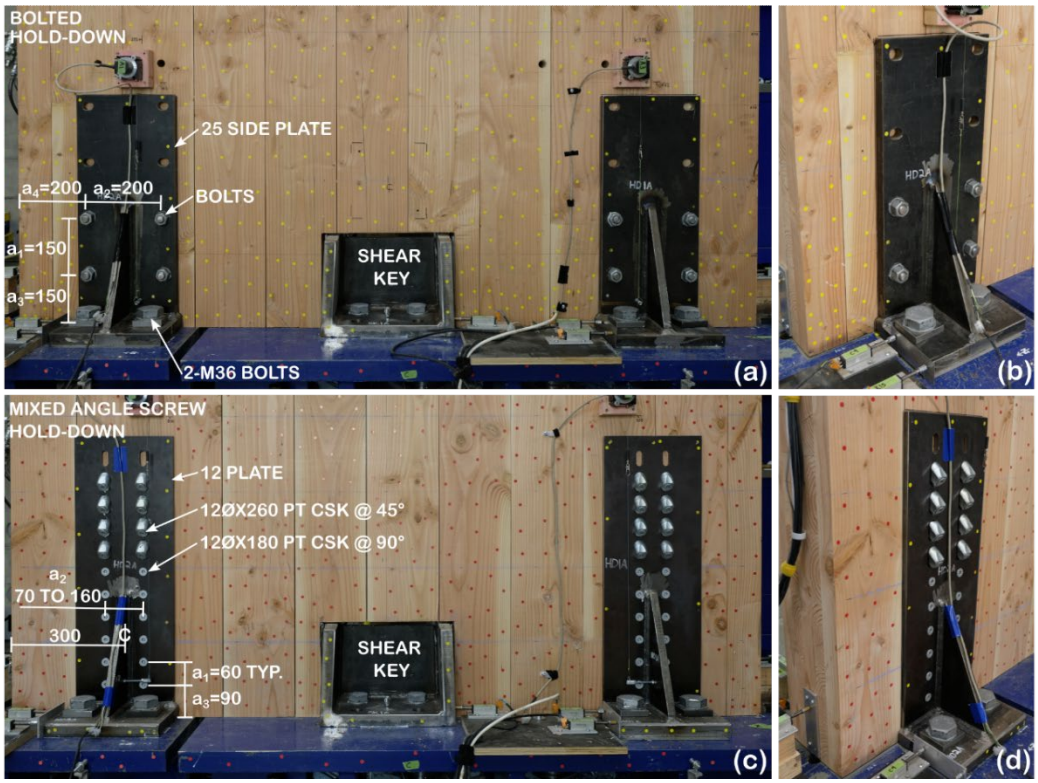

Figure 4: Hold-down details: (a,b) bolts and (c,d) mixed angle screws.

A typical steel shear key was installed in a 250x350mm rectangular notch at the base of the wall to resist base sliding through steel-to-timber bearing onto the cross layers, as shown in *Figure 5*. Most wall specimens used one shear key, but the longest walls (W11 and W12) were provided with two because of their inherently greater shear capacity due to the low aspect ratio of 0.52. A 3mm gap was provided on each side of the shear key for assembly tolerance, and shimmed tight with steel plates to create a tight fit (i.e. minimize initial slip). The steel side plates were sloped at 2.5% (*Figure 5b*) to prevent binding when the wall base rotated. Each shear key's plates, welds, and bolts were designed to resist a lateral demand of 500kN resulting from a uniform bearing stress of

$f_{c,0}$=30MPa in the cross layers at the steel-to-timber contact surface. To capture the base response of the wall, a series of vertical spring potentiometers were used to determine the base rotation while lateral spring potentiometers measured the sliding of the base, as seen in *Figure 6*. Linear potentiometers were placed on the front surface of the wall to evaluate the curvature and shear strain profiles of each wall panel. These were installed at the mid-height of walls loaded at a height of 2.6m and at third points over the height of the walls loaded at a height of 6.6m.

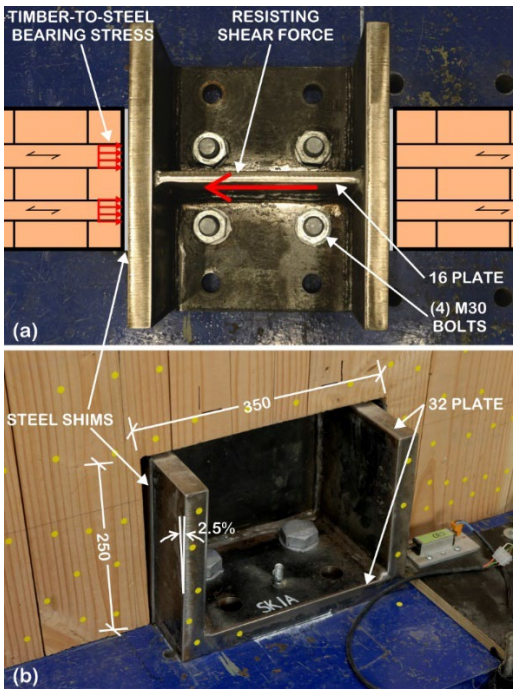

Figure 5: Steel shear key details: (a) plan view and (b) isometric view.

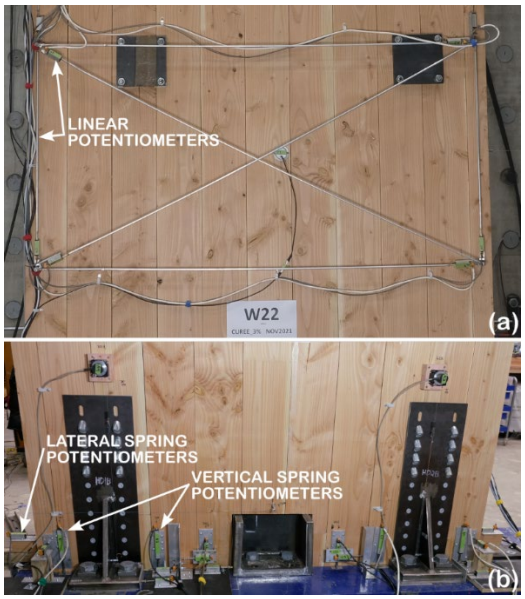

Figure 6: Typical wall instrumentation: (a) linear potentiometers for CLT panel strains and (b) spring potentiometers for base sliding or rotation.

2.4 Test results and discussion

Plots of the global load vs. drift curves and base moment vs. base rotation curves are shown in *Figure 7*. *Table 3* lists key test results including initial stiffness, yield strength and displacement, maximum strength and displacement, ultimate strength and displacement, and ductility. The yield point for each specimen was determined using the methodology described in the testing standard *EN12512* [24]. An additional y-axis is shown for the moment vs. base rotation plots to represent the quasi-uplift force demand on the HD subjected to tension force, calculated with Equation *(2*). The hysteretic loops were severely pinched and therefore had a reduced amount of energy dissipation compared with elastoplastic hysteretic behaviour. A significant portion of the global drift was due to rotation of the wall base.

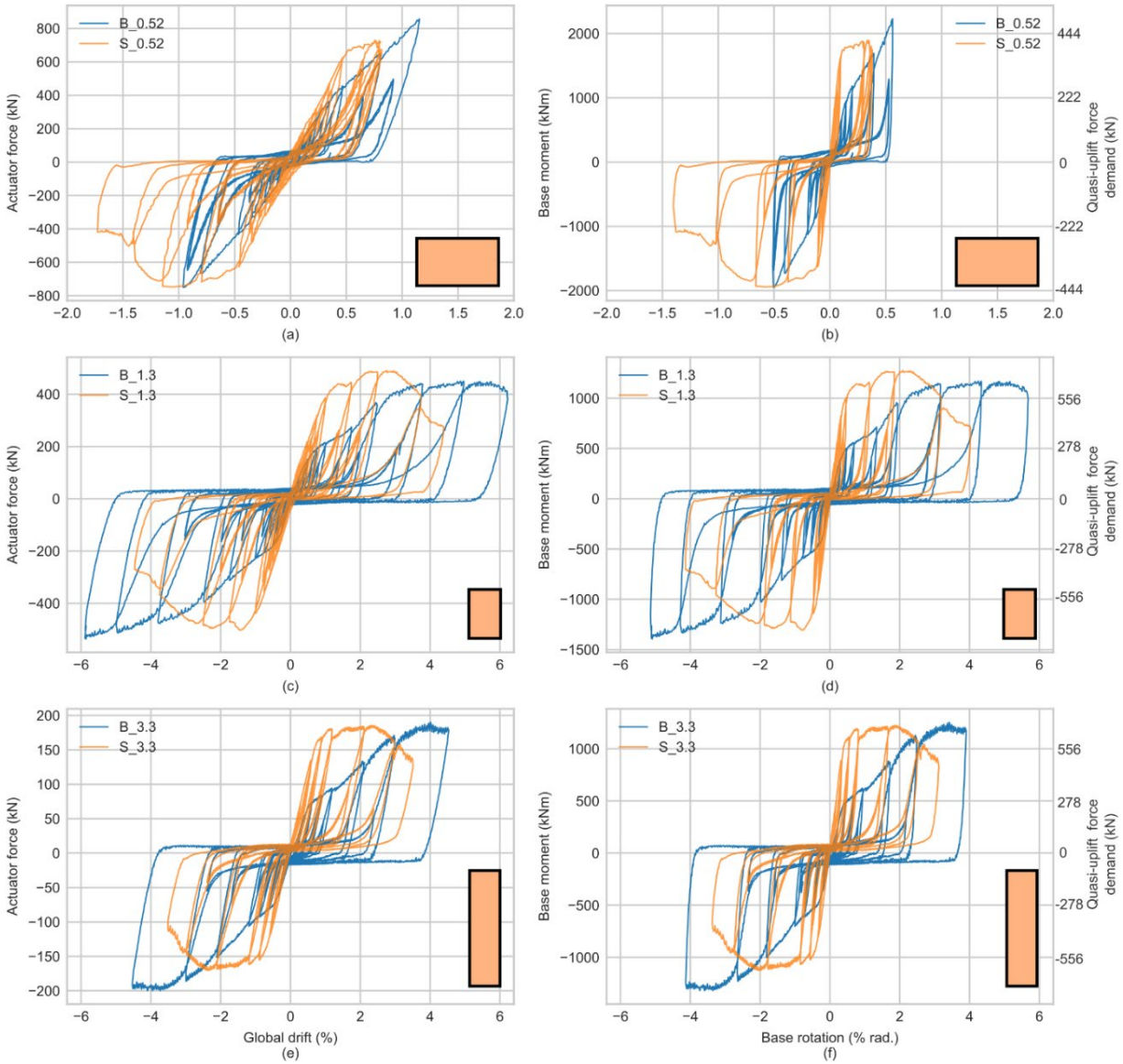

Figure 7: Global hysteretic behaviour (left) and base moment vs. rotation (right) for walls with aspect ratios of: (a,b) 0.52, (c,d) 1.3, and (e,f) 3.3.

Table 3: Summary of key test results.

Test ID	Stiffness (kN/mm)		F_y (kN)		F_{max} (kN)		D_y (% drift)		D_{Fmax} (% drift)		Ductility, μ (D_u/D_y)	
	pos	neg	pos	neg	pos	neg	pos	neg	pos	neg	pos	neg
B_0.52	40.1	-37.6	374	-316	*857*	*-750*[b]	0.34%	-0.31%	1.16%	-0.96%	-	-
S_0.52	46.0	-46.4	675	-647	*721*	-748	0.52%	-0.49%	0.77%	-1.08%	-	2.8
B_1.3	11.4	-15.3	182	-170	450	-536[b]	0.58%	-0.39%	4.96%	-5.86%	(10)[c]	(15)[c]
S_1.3	14.7	-18.4	398	-423	490	-503	0.95%	-0.84%	2.76%	-1.46%	3.9	4.2
B_3.3	2.4	-1.9	73	-76	190	-200[b]	0.53%	-0.47%	4.02%	-4.10%	(7.6)	(9.6)
S_3.3	3.3	-3.3	161	-138	185	-170	0.69%	-0.66%	2.31%	-2.38%	4.3	4.8

The wall specimens with bolted HDs did not achieve their ultimate strength. Wall B_0.52 buckled while walls B_1.3 and B_3.3 reached maximum interstorey drifts of 4.5% and 6% (maximum uplift of 88mm at HD), respectively, which were the upper limits for their test setups. The HD bolts yielded in bending, then progressively gained strength due to significant "rope effect", but no ultimate brittle failure mode occurred to cause ultimate strength loss. However, the failure mode of the bolted HDs was ductile. The displacement ductility values ($\mu=D_u/D_y$) were not obtained for these tests but were instead calculated as D_{max}/D_y and reported in parentheses.

Damage observation

Damage to the CLT walls was concentrated exclusively at the HD fasteners and in the bottom CLT panel corners (i.e. wall toes), where crushing occurred. No splitting or crushing was observed around the shear key notches. The wall base of each specimen, except for B_0.52 and S_0.52, is shown in *Figure 8* when their maximum positive drift was reached. While the aspect ratios differed, the specimens with the same HDs exhibited very similar damage at their bases and in their HD fasteners.

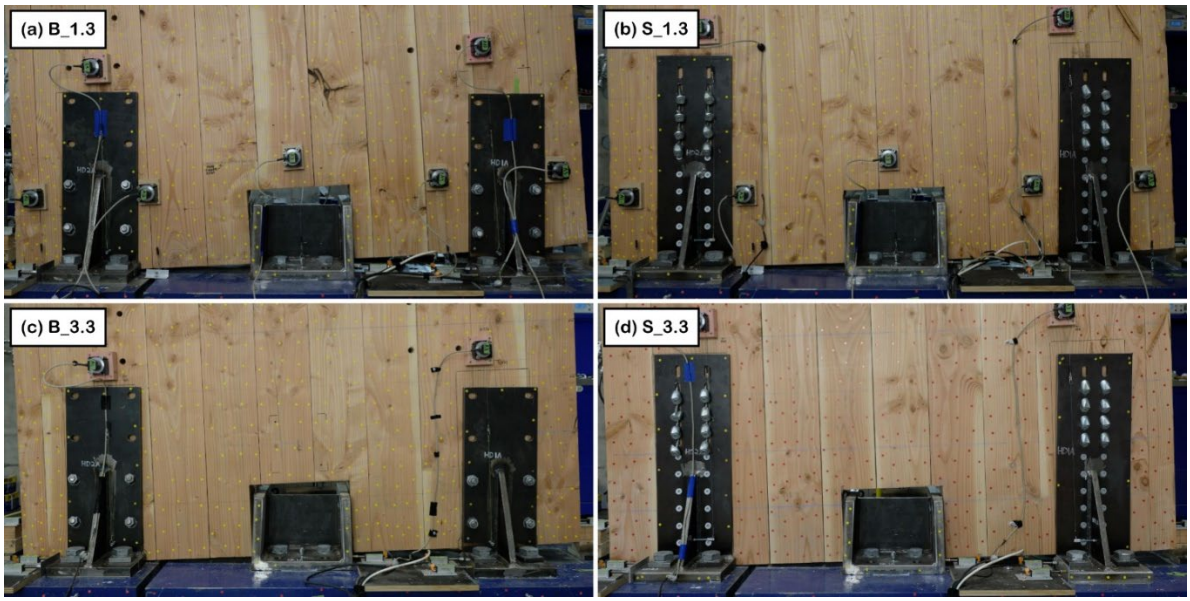

Figure 8: Wall bases at maximum positive drift level.

Representative damage in the bolted HDs of specimens B_1.3 and B_3.3 is shown in Figure 9a and a section view through a typical bolt is shown in Figure 9b. The timber material below the bolt crushed and four plastic hinges were formed as the bolt was progressively bent to a greater degree. Due to flexural yielding of the bolts, residual uplift at the HDs (and therefore residual wall drifts) were observed in each test with bolted HDs. Some layers of the CLT panel around the bolted connection showed local shear or splitting damage due to bolt embedment but no ultimate brittle failure modes (row shear, group tear-out, or net tension fracture) occurred to cause significant strength loss in the system. Ultimate failure of bolted and dowelled timber connections typically occurs because of a brittle failure mode in the timber. With adequate edge distances and spacings, brittle failure modes will be delayed until significant displacement causes a mode cross-over, as observed in dowelled CLT connections tested by Ottenhaus et al. [21]. The bolt spacings in this study were evidently adequate to achieve ductile behaviour in the bolted HD without mode crossover at the imposed displacement levels. Typical damage to the mixed angle screwed HDs is shown in Figure 9c. Screws removed after completion of the test are shown in Figure 9d. As the HDs were subject to gradually larger uplift forces, the inclined screws progressively pulled out from the timber in a ductile manner, rather than fracturing. The 90° screws developed plastic hinges as they were bent and also pulled out of the timber due to significant “rope effect”. In addition to the damaged observed at the HD connections, the toes of each wall base corner in all tests were moderately crushed due to a concentration of compressive stress, as shown representatively in *Figure 10*.

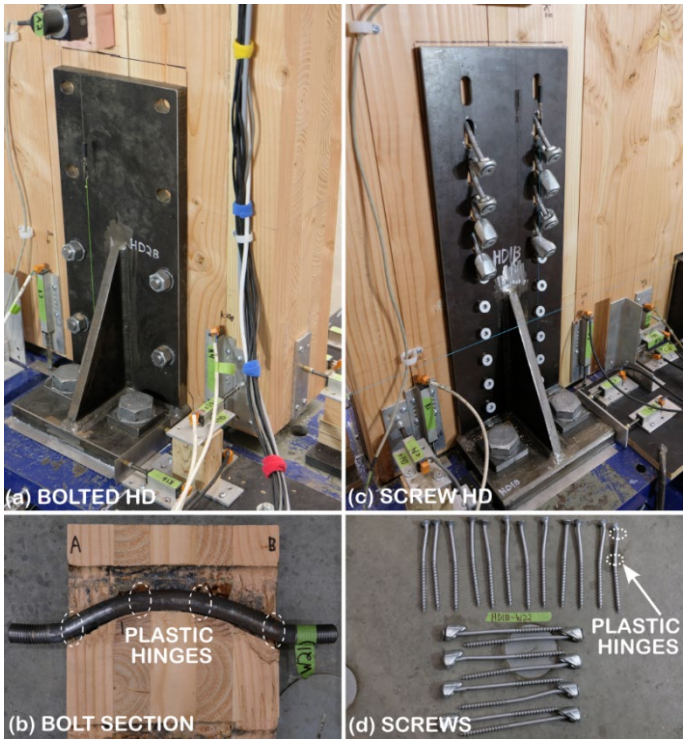

Figure 9: Damage observed: (a,b) bolted hold-down and (c,d) mixed angle screw hold-down.

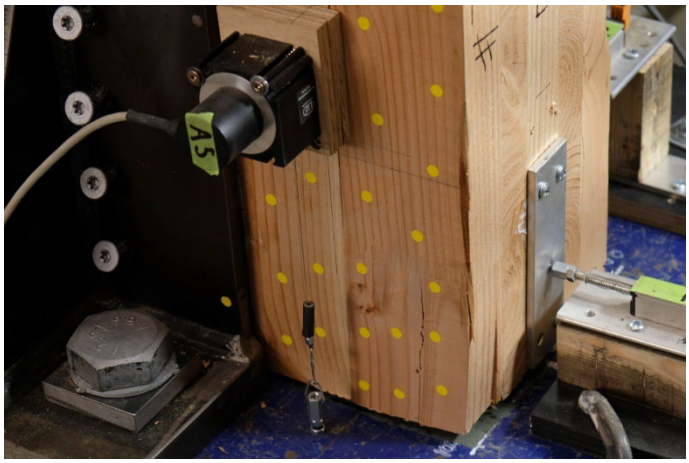

Figure 10: Typical crushing damage observed at CLT wall toe.

No brittle failure modes were observed in the regions around the HDs although significant tensile stress concentration occurred in the local region above each HD. The spacings and edge distances used by the bolted and mixed angle screw HDs were adequate to prevent brittle failure modes. Accurate prediction of the brittle failure modes at the corners of CLT walls is a significant gap in the current research literature and needs further investigation, particularly as the capacity of HD connections increases.

Long wall buckling

The long walls (B_0.52 and S_0.52) exhibited buckling out-of-plane prior to reaching their peak strengths and the tests were stopped when the failure mode was observed. However, one exception occurred, as wall S_0.52 was able to achieve post-peak behaviour without significant buckling behaviour in the negative loading direction. *Figure 11* shows the applied forces and deformed shape when out-of-plane buckling of the long walls occurred. This buckling mode was unexpected and has not been considered or observed in previous analytical or experimental research on CLT walls. It could be mitigated by providing more out-of-plane restraints at the top and bottom edges of the wall, such as a continuous floor diaphragm with strong and stiff connections. However, the results of these tests show that further investigation is required to adequately assess such failure modes and determine minimum strength and stiffness requirements for out-of-plane restraints and their connections to prevent the orthotropic CLT plates from buckling under in-plane loads.

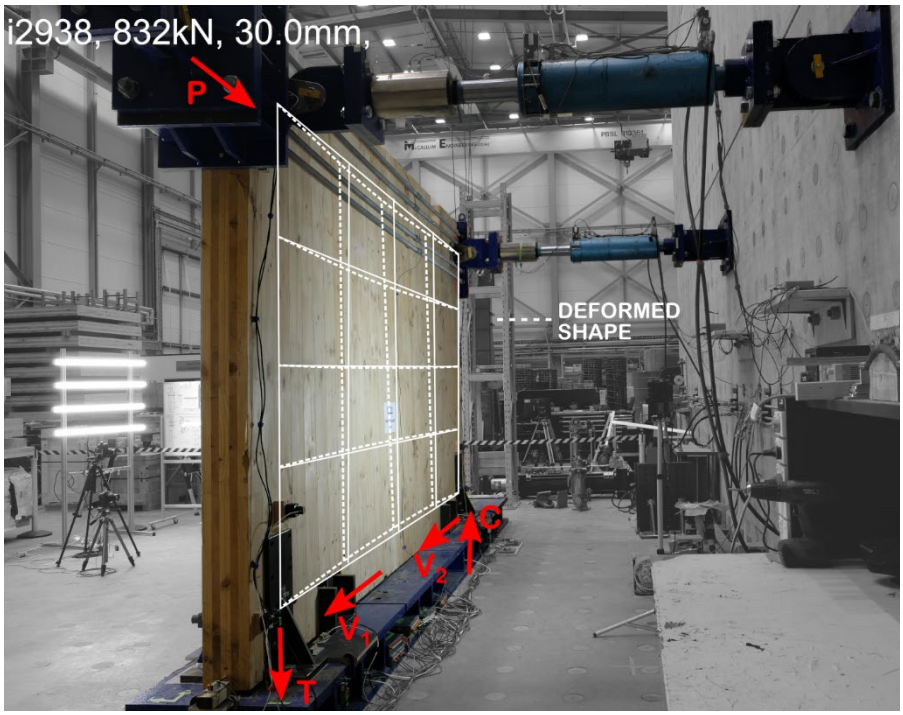

Figure 11: Buckling mode observed for long CLT wall specimens B_0.52 and S_0.52.

Wall system overstrength

System overstrength factors for the wall specimens were calculated according to Equation *(3)*. These factors were determined only for the walls with mixed angle screwed HDs because, as previously discussed, the walls with bolted HDs did not reach their ultimate strength. However, ratios of maximum experimental moment to nominal base moment were calculated and reported in parentheses for the walls with bolted HDs in *Table 4*.

$$\gamma_{exp} = M_{max}/M_n \qquad (3)$$

where M_{max} is the maximum base moment applied during the experiment
M_n is the predicted nominal base moment strength (i.e. strength reduction factor Ø=1 in NZS3603 [22] or partial factor γ_m=1 in Eurocode 5 [6])

The wall base moment capacities were determined with the design method from Schickhofer et al. [25], which uses a rectangular stress block in the compression zone. The bolted HD strengths were determined using the European Yield Model equations from Eurocode 5 [6] and the mixed angle screw HD strengths were found by the addition of strengths for the 90° and 45° screws. The calculated nominal strengths, maximum experimental demands, and overstrength factors for each specimen are summarized in *Table 4*.

Table 4: Nominal base moment strength and corresponding experimental overstrength factors

Test ID	Calculated nominal HD uplift strength, T_n	Maximum experimental quasi-uplift force demand, T'_{max}	Calculated nominal base moment strength, M_n	Maximum experimental base moment, M_{max}	System overstrength, γ_{exp}
	(kN)	(kN)	(kNm)	(kN)	
B_0.52	206	496	967	2230[a]	(2.3)[c]
S_0.52	262	431	995	1940	2.0
B_1.3	310	772	517	1390[b]	(2.7)[c]
S_1.3	523	728	705	1310	1.9
B_3.3	310	733	517	1320[b]	(2.6)[c]
S_3.3	523	678	705	1220	1.7

a) Wall buckling occurred and the test was terminated.
b) Peak strength not reached because maximum displacement in test setup reached.
c) Calculated with maximum experimental base moment instead of peak value because peak strength was not reached.

The wall system overstrength factors increased with lower height-to-length aspect ratios. The larger shear force components of the squat walls had proportionally higher surface friction at the shear key bearing interfaces which acted as additional HD forces to the wall system. This source of overstrength can therefore be attributed to the analytical method used to calculate the wall base moment capacities which neglected the overturning resistance contribution of any shear transfer connection (e.g. the shear key).

System overstrength of the walls with bolted HDs could not be derived because they did not reach their peak strength due to the stroke limit of the test setup and an absence of brittle failure modes. Although these specimens did not reach their peak strengths, walls B_1.3 and B_3.3 imposed significant local ductility demands on their HDs of 21 and 14, respectively, at their maximum displacements. These values will likely exceed the local ductility demand on the connection when designing a CLT shear wall for seismic demands. Therefore, it is reasonable to use an overstrength value less than the largest value found in these experiments (2.7) if the local ductility demands are low enough and are adequately predicted by the analytical model of the designer.

Aspect ratio influence on high-capacity CLT walls

Rigid body behaviour was also dominant in the CLT walls tested in this study but the in-plane deformations were not always negligible, particularly at the yield point.

Figure 12 describes the relative contributions of the four deformation sources (d_b=bending, d_v=shear, d_{sl}=base sliding, d_{ro}=base rotation) to the global drift at the yield, peak, and ultimate points. The deformation values are summarized numerically in *Table 5*. The contribution magnitudes were similar in the positive and negative directions and were averaged to produce

each bar plot component (and each value in *Table 5*). The tests with bolted HDs did not reach their ultimate point, therefore, these points are not shown.

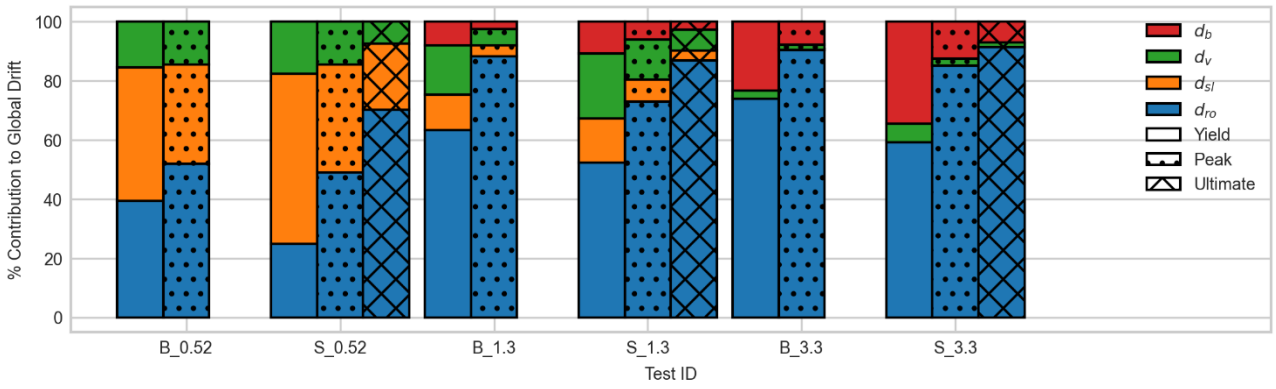

Figure 12: Deformation contributions to global drift at yield, peak, and ultimate force points.

Table 5: Deformation contributions at yield, peak, and ultimate force points.

	Yield				Peak				Ultimate			
Test ID	**d_b (mm)**	**d_v (mm)**	**d_{sl} (mm)**	**d_{ro} (% rad)**	**d_b (mm)**	**d_v (mm)**	**d_{sl} (mm)**	**d_{ro} (% rad)**	**d_b (mm)**	**d_v (mm)**	**d_{sl} (mm)**	**d_{ro} (% rad)**
B_0.52	0.0	1.3	3.9	0.13%	0.0	3.9	8.9	0.53%	-	-	-	-
S_0.52	0.0	2.2	7.2	0.12%	0.0	3.4	8.4	0.44%	0.0	2.6	8.0	0.96%
B_1.3	1.0	2.1	1.5	0.31%	3.5	7.8	5.3	4.78%	-	-	-	-
S_1.3	2.2	4.6	3.1	0.41%	3.1	7.1	3.8	1.46%	2.5	6.6	3.0	3.12%
B_3.3	7.3	0.8	-0.2	0.36%	20.2	4.5	-0.8	3.59%	-	-	-	-
S_3.3	14.6	2.7	0.0	0.38%	18.7	3.6	-1.3	1.95%	14.1	2.9	-2.1	2.79%

a) d_b and d_v are the lateral deflections at the loading point due to CLT panel bending and shear, respectively
d_{sl} is the amount of wall base sliding
d_{ro} is the amount of base rotation

The longest walls, with an aspect ratio of 0.52, had the greatest amount of sliding and shear deformation contributions. Shear deformation is typically negligible in conventional CLT walls but in this case it contributed nearly 20% of the total drift observed at the yield and peak points. The tallest walls (B_3.3 and S_3.3) had negligible base sliding but quite significant bending-induced deformation. Base rotation was still a dominant source of deformation in all six specimens and its contribution to the total drift increased from the yield point to the ultimate point because this kinematic mode is the only one affected by progressive failure of the HD and its uplift displacement.

The aspect ratio of CLT shear walls in a seismic LLRS is restricted in national design standards such as SDPWS [3]. Greater levels of ductility and force reduction are available for the design of CLT walls when their height-to-length aspect ratio is between 2:1 and 4:1 (or between 1:1 to 4:1 in the proposed Italian provisions) to promote a base rotation mechanism, which is preferred instead of sliding. However, the long walls in this study with an aspect ratio of 0.52:1 exhibited a base

rotation failure mode because the shear keys were strong enough to prevent base sliding. The base rotation mechanism is evident in Figure 12 as the contribution of base rotation progressively increased from the yield to the ultimate point in walls B_0.52 and S_0.52. Therefore, although the geometry of a CLT wall is a factor in determining its capacity, it is the relative strength of the base connections that determine its failure mechanism rather than exclusively its aspect ratio. Instead of restricting the aspect ratio of cantilever CLT shear walls, it is more reasonable to instead require a failure mechanism dominated by base rotation and ductile HDs with an adequate level of local ductility. By restricting the use of long walls, structural designers are unable to take advantage of their inherently greater stiffness and lower yield point which will help limit interstorey drifts when compared to more slender, tall CLT walls.

The CLT walls with high aspect ratios had greater ductility factors (*Table 3*), but it should be noted that the factors were calculated with ultimate displacements which were achieved at drifts exceeding 2.5%, a common upper bound for the ultimate limit state (ULS) used in seismic design. If limited by the 2.5% drift limit, the tallest walls, B_3.3 and S_3.3, would have modified ductility values of 5.0 and 3.7, respectively. Therefore, the greater ductility of walls with high aspect ratios may need to be practically reduced for seismic design if their stiffness is inadequate.

Energy dissipation

The energy dissipated and equivalent viscous damping (EVD) are plotted for each primary cycle and its two trailing cycles in *Figure 13*. The solid lines show the primary cycles, dashed lines are the first trailing cycle, and the dash-dotted lines are the second trailing cycle. The EVD for each wall specimen was calculated using Equation *(4)*. It should be noted that the walls with bolted HDs did not reach their ultimate displacements and therefore the final data points in *Figure 13* are not representative of post-peak behaviour.

$$\xi = \frac{E_{cycle}}{2\pi F_{max} D_{max}} \qquad (4)$$

where E_{cycle} is the energy dissipated in the full cycle

F_{max} is the maximum actuator force reached

D_{max} is the maximum actuator displacement reached

ξ is the equivalent viscous damping

The EVD in the primary cycles was between 10 and 18%, except for the final cycle of B_0.52 when the specimen experienced a buckling failure. The lower EVD of the trailing cycles compared to the primary cycles in each test indicates significantly reduced energy dissipation after damage occurred in the primary cycle. This phenomenon can also be observed in the global hysteresis of

the specimens in *Figure 7* as the trailing cycles produced more severely pinched loops with less energy dissipation (i.e. smaller area enclosed by the trailing cycle loops). The reduction of EVD in the trailing cycles was the greatest for the walls with mixed angle screw HDs.

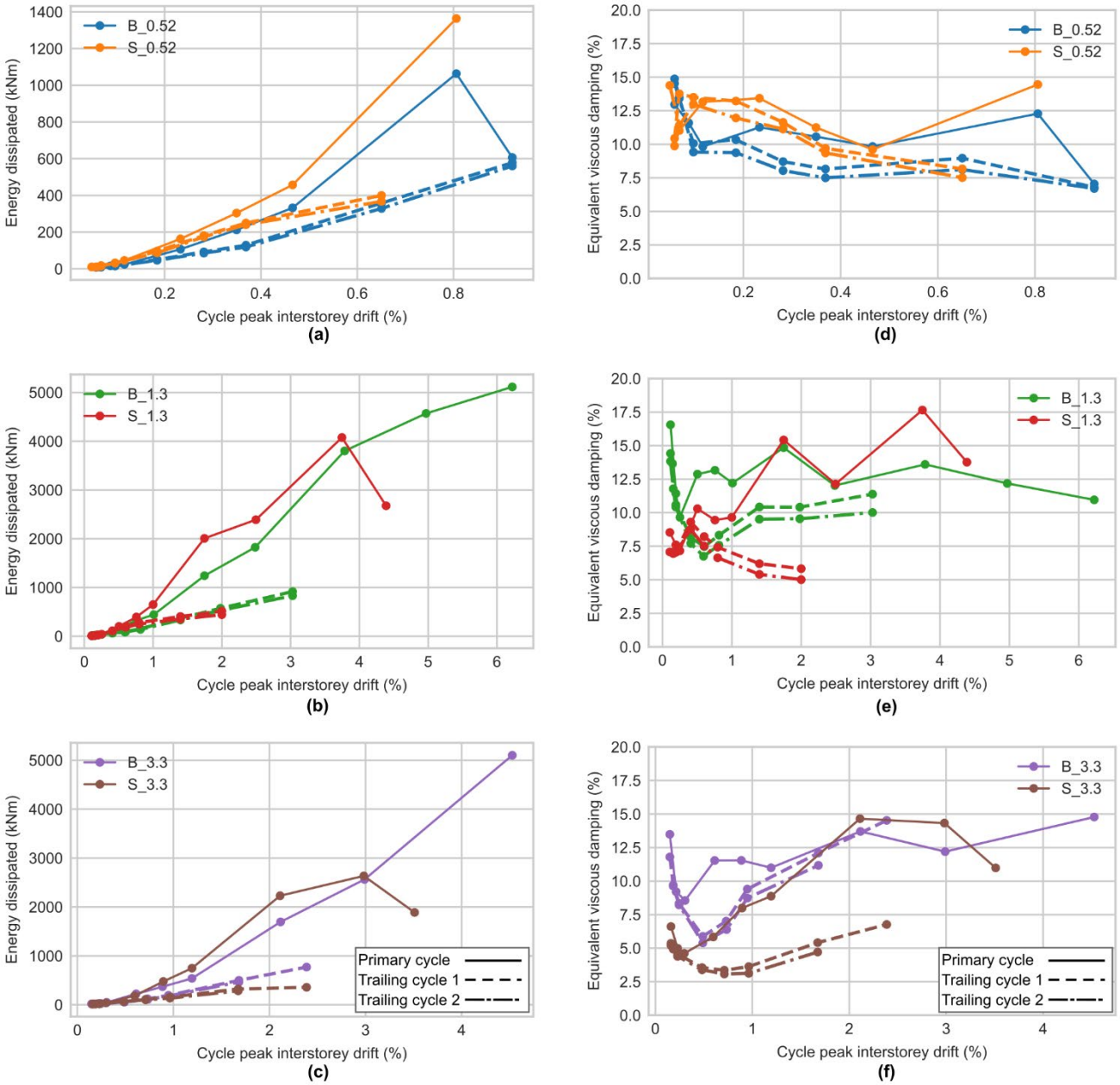

Figure 13: Energy dissipated in full cycles (a, b, c) and equivalent viscous damping (d, e, f).

Comparison to conventional CLT shear walls

Table 6 lists the comparisons between the tested walls and the conventional CLT wall test results previously summarized in Table 1. Specimens B_1.3 and S_1.3 had a similar aspect ratio and loading height compared with several of the conventional CLT walls and demonstrated greater stiffness than all the conventional CLT wall test results, which had a mean stiffness of 4.4kN/mm.

The peak lateral force of specimen S_1.3 was 163% greater than the strongest conventional wall (specimen CB-SN-14 by Popovski and Karacabeyli [12] with F_{peak}=191kN). The strength utilization values of the specimens in this study exceeded those calculated for the conventional CLT wall test results and even exceeded 100% for three of the wall specimens, indicating their theoretical nominal strength was slightly exceeded, which should not occur if capacity design principles are followed.

It should be noted that most of the conventional walls described in Table 1 included additional vertical load which enhanced their strength and stiffness, while the experiments in this study only included the incidental vertical load from the self-weight of actuators and fittings. Additional vertical load would further enhance the lateral capacity of the high-capacity CLT shear walls.

Table 6: Summary of high-capacity single CLT wall test results for comparison to past conventional CLT wall tests.

Specimen ID	**CLT wall dimensions T x L x H**	**Aspect Ratio**	**CLT Grade**	**Stiffness, k_i (kN/mm)**	**Maximum lateral force, F_{peak} (kN)**	**Strength utilization, λ**	**Quasi-uplift force demand, T' (kN)**
B_0.52	205 x 5000 x 2600	0.52	SG8 primary layers / SG6 cross layers	38.9	857	69%	495
S_0.52	205 x 5000 x 2600	0.52		46.2	748	60%	432
B_1.3	205 x 2000 x 2600	1.3		13.4	536	111%	774
S_1.3	205 x 2000 x 2600	1.3		16.6	503	104%	727
B_3.3	205 x 2000 x 6600	3.3		2.2	200	105%	733
S_3.3	205 x 2000 x 6600	3.3		3.3	170	89%	623

3. COUPLED WALL TESTS

3.1 Couple wall specimen

As shown in *Figure 14*, the coupled CLT wall consisted of two CLT wall panels linked by three steel beams. The specimen geometry, CLT elements, and steel beams were chosen based on a 2/3-scale preliminary seismic design of a 6-storey building located in Christchurch, a moderate-to-high seismic region in New Zealand, with a storey height of 3m, seismic weight of 4kPa, tributary area of 320m^2, and a degree of coupling β=0.5. The equivalent static method from the New Zealand seismic design standard (NZS1170.5 [26]) was used to determine the design forces with an assumed ductility factor of 4, approximate fundamental period of T_1=0.6 seconds (assumed T_1≈0.1N, where N is the number of storeys, per ASCE 7-22 [27]), Normal Importance, and shallow soil (class C).

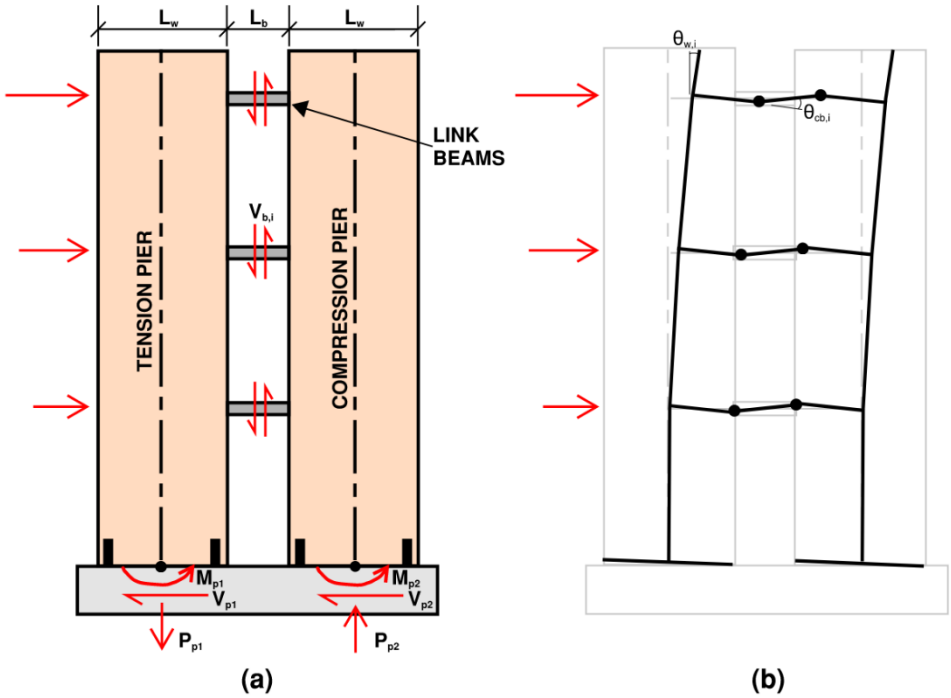

Figure 14: Hybrid coupled CLT wall system with link beams: (a) general configuration with free-body diagram and (b) intended plastic mechanism.

The coupled CLT wall specimen is shown in *Figure 15*. The specimen was composed of two 2000mm long 5-ply (45/35/45/35/45) CLT wall piers and 850mm long 200UB18 steel link beams between the piers. The CLT was composed of New Zealand Douglas Fir with longitudinal layers of 45x190mm SG8 boards and cross layers of 35x140mm SG6 boards, where SG8 and SG6 are timber grades used in the New Zealand Timber Structures Standard [22]. SG8 grade timber has an average modulus of elasticity (MOE) 8GPa and SG6 grade timber has MOE 6GPa. The measured

mean density was 484kg/m^3 with a COV of 0.12 and the mean moisture content was 11.4% with a COV of 0.072.

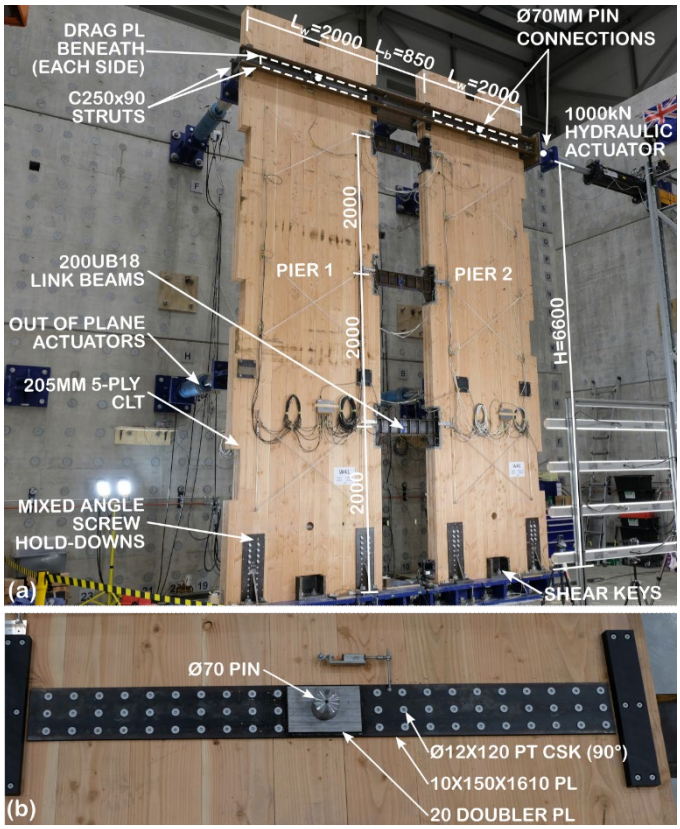

Figure 15: The coupled CLT wall specimen: (a) overall and (b) drag plate beneath channel struts.

3.2 Experiment setup and loading protocol

The coupled wall was loaded by a 1000kN-capacity hydraulic actuator at a height of 6600mm. The actuator was connected by a Ø70mm pin to a pair of symmetric C250x90 channel struts which transferred the load to symmetric drag plates *(Figure 15b*) on each wall pier through Ø70mm pins. A series of out-of-plane actuators were connected to the specimen by pinned connections with spherical bearings to provide transverse stability while allowing in-plane displacement of the specimen. No additional gravity load was applied to the specimen, however, gravity load on the wall piers may be present in a real building and must be considered in design.

Symmetric mixed angle screwed HDs (*Figure*), based on the experiments by Wright et al. [20], were used on both sides of each wall pier base (i.e. 4 HDs per pier). Each HD used 8-Ø12x260mm and 12-Ø12x180mm self-tapping screws installed at 45° and 90°, respectively. The 45° screws were installed so that they were engaged mainly in tension when the HDs were uplifted. Each screw was partially threaded to 100mm from the tip and had a countersunk head. The 45° screws were each fitted with an inclined washer and installed into a vertically slotted hole in the steel plate.

A steel shear key (*Figure 16a*) was installed at mid-length of each wall pier in a 350mm by 250mm full-thickness rectangular notch to provide base shear resistance. The keys were installed with a tolerance gap of approximately 3mm on each side and shimmed with steel plates to achieve a tight fit. The contact surfaces on each side were angled at 2.5% to prevent binding as the wall pier bases rotated. The shear keys and HDs were bolted to steel base fittings which were bolted to the strong floor.

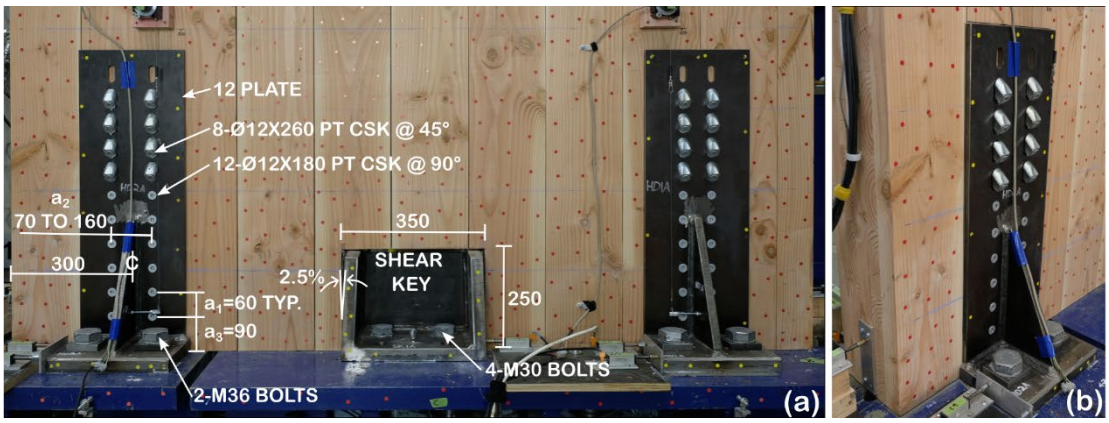

Figure 16: Wall pier base connections: (a) front elevation and (b) isometric.

As shown in *Figure 17*, 200UB18 steel link beams were connected to each CLT panel with a capacity-designed screwed end plate connection, based on the results of connection experiments. A stiffened 20mm end plate was welded to each side and 16-Ø12x350mm fully threaded screws with countersunk heads were installed into Ø8mm pre-drilled holes in the CLT panel edges. Each end of the link beams was installed in a 110mm by 570mm rectangular notch with approximately 10mm thick cementitious grout poured between the steel and the CLT elements to create a tight connection. The CLT surface adjacent to the cementitious grout was painted with a waterborne paint to seal the timber surface and prevent water loss from the grout while curing. The beams' webs were stiffened with 6mm by 40mm stiffeners spaced at 150mm, following the stiffener requirements for active eccentric braced frame links in the New Zealand Steel Structures Standard NZS3404 [28].

The effective length (e), nominal shear strength (V), and moment strength (M), are used to determine the governing failure mode of an active steel link beam in EBFs by calculating the eV/M ratio. According to the NZS3404 Standard [28], link beams with eV/M≤1.6 are *shear-critical*, eV/M≥3.0 are *flexure-critical*, and elements between these bounds are *intermediate*, as they will experience a combination of failure modes. Similar definitions are used in the American Steel Design Standard AISC 341 [29], but a limit of eV/M≥2.6 is used to delineate between *intermediate* and *flexure-critical* link beams. The effective length of the link beams in the test specimen was e=750mm (measured between the ends of its central stiffener plates) and the corresponding ratio

of eV/M was 2.2, based on the nominal shear (V) and moment (M) capacities. Therefore, the links were *intermediate* and theoretically governed by a combination of shear and flexural yielding. The steel link beams were fabricated from 200UB18 I-beams made from seismic grade 300-SO steel, following the hot-rolled steel production standard AS/NZS 3679.1 [30].

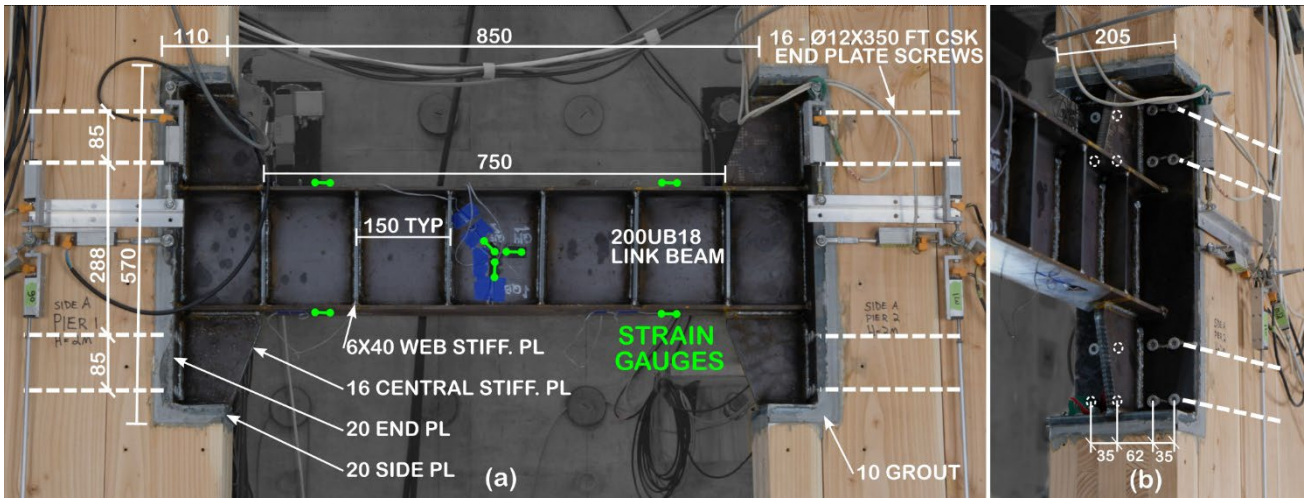

Figure 17: Typical steel link beam (200UB18) between CLT walls: (a) elevation and (b) screwed end plate connection.

Each steel beam had seven strain gauges attached to the steel surface, as shown in Figure a. Four gauges were installed on the flanges to determine the curvature at two locations near the beam ends and three were placed in the central web panel zone arranged in a 0/45/90 rosette configuration to observe the web panel strains.

Primary instrumentation on the CLT panels is shown in *Figure* . Sixteen linear potentiometers were installed on the front surface of each CLT pier to capture their in-plane curvature and shear strain profiles. Eight 100mm spring potentiometers were installed at the bottom edges to capture base rotation and uplift. The base rotation and neutral axis depth of each pier were determined at all load steps by fitting linear functions through the vertical displacement readings from the vertical spring potentiometers along the base. Additional secondary instrumentation was also installed to monitor the beam connections, movement of the steel bases, and other connections along the load path.

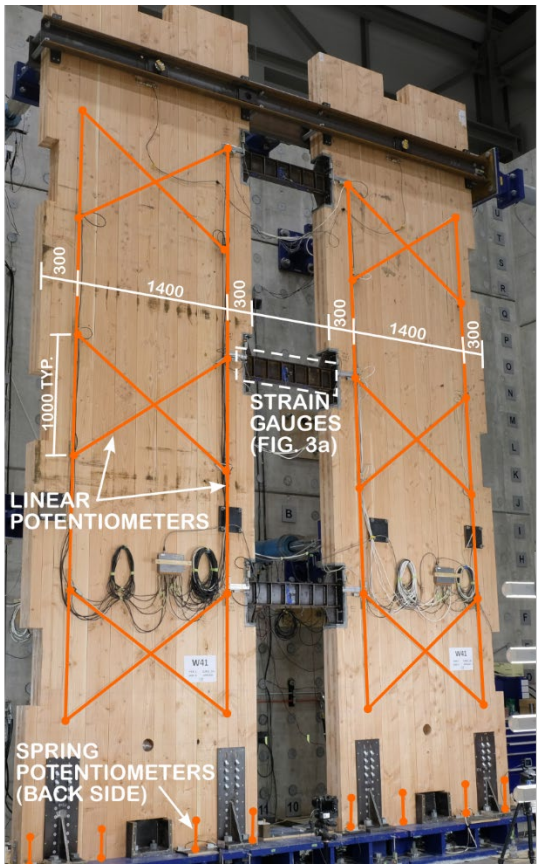

Figure 18: Primary instrumentation installed on coupled CLT wall specimen.

The CUREE loading protocol [23] was used to define the series of displacements imposed on the specimen. A reference displacement of D_{ref}=198mm, or 3% global drift, was chosen based on preliminary pushover analyses and available component properties. As shown in *Figure 19*, The experiments were terminated at a maximum drift of +/-4.5% due to limited actuator displacement capacity.

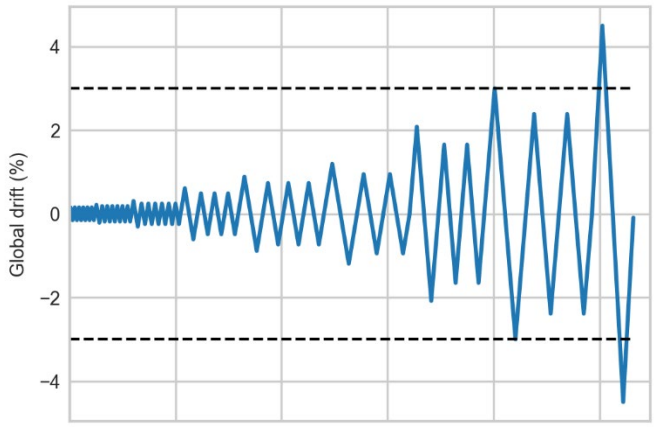

Figure 19: Example of CUREE loading protocol with D_{ref}=198mm (3% global drift).

3.3 Test results and discussion

Damage observations

Damage observed in the specimen was concentrated in three locations: (1) the steel link beams, (2) screws in the HDs, and (3) compression toes of each CLT pier. The progression of damage initiation is illustrated in *Figure 20* with the corresponding peak drift of the cycle in which the damage initiated.

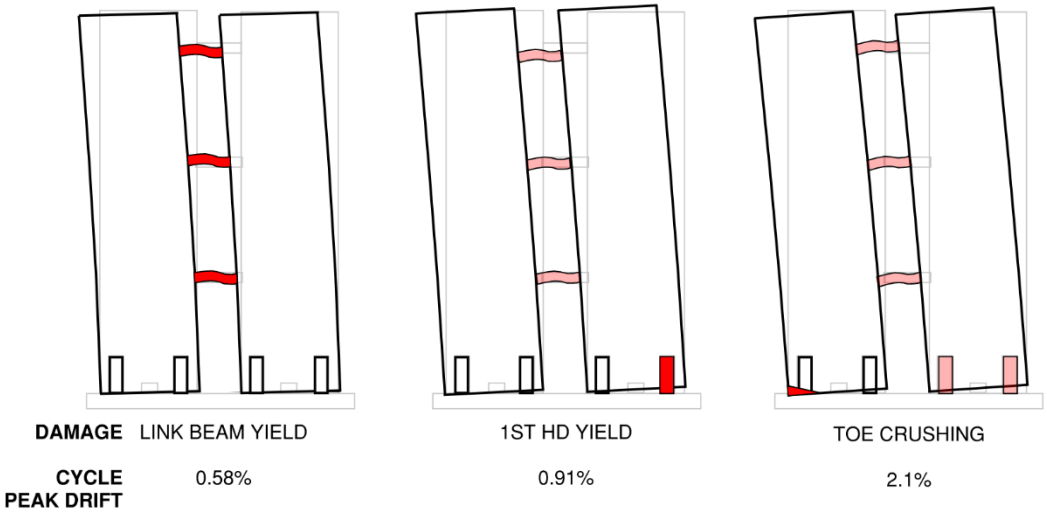

Figure 20: Progression of damage initiated in the coupled CLT wall specimen and corresponding peak drift of the cycle in which the damage initiated.

Figure a shows a representative steel link beam after the cyclic testing was completed. Mill scale flaking on the beam webs occurred as the system yielded and indicated the onset of yielding in the link beams. The link beams installed at heights of 2m and 4m each showed one instance of fillet weld fracturing at the stiffener plate-to-flange joint during the final 4.5% drift cycle. However, it was observed after the test that the fillet weld legs in these regions were only 4mm wide, not the specified 6mm, and showed poor penetration of the base metal. Therefore, this failure mode was due to an inadequate amount of weld material applied to the joint and inadequate quality control of the welding process (e.g. improper technique or welding parameters) which caused poor penetration. Inelastic buckling of the link beam webs and flanges also occurred and eventually fracture occurred in these regions, due to low-cycle fatigue.

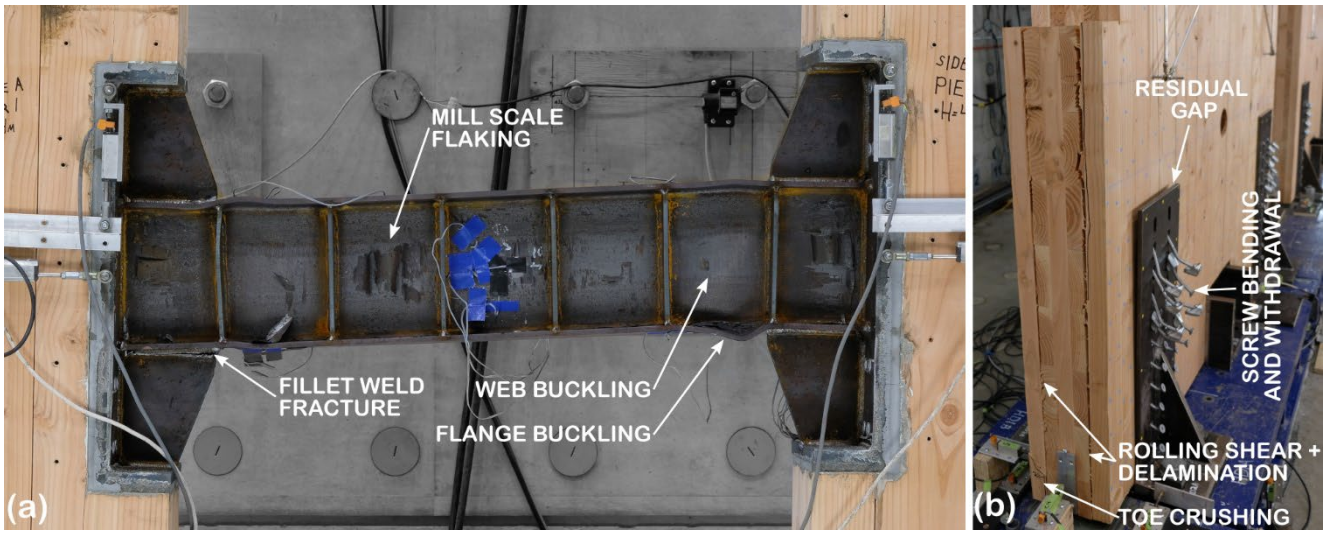

Figure 21: Post-test damage observed for the (a) link beam and (b) mixed angle screw HD.

The HD screws, shown in *Figure 21b*, progressively bent and withdrew from the CLT. Although the HDs experienced uplift displacement demands up to 116mm, no screw fracturing was observed during or after the tests. Prying of the HD side plates away from the CLT surface was observed due to the cumulative local bending moments applied to the side plates by the screws engaged in bending. The gap between the top of the HD side plate and adjacent CLT surface reached a maximum of 30mm when the specimen was subjected to its peak load. A residual gap of 6 to 12mm was present *(Figure 21b*) after the test was completed, indicating flexural yielding occurred in the HD side plates due to the prying action.

The exterior edge of pier 1 experienced a combined rolling shear and delamination failure of one board in each of the panel's outer layers due to a concentration of compression force at the toe. The delamination initiated in the 2.1% drift cycle and became more severe until fully delaminating in the final 4.5% drift cycle. This failure mode is directly related to the presence of a notch located above the delamination (*Figure 21b*) which created a discontinuity in the CLT panel and promoted the local delamination. The exterior edge of pier 2 also showed local delamination initiating near the toe, but it was not as severe and full delamination did not occur.

Global behaviour

Figure 22a shows a plot of the global drift versus force. Global drifts were calculated by dividing the actuator displacement by the loading height of 6600mm. The hysteresis loops were "pinched", causing a reduction of the total energy dissipation, and the degree of pinching was greater as the peak drift magnitudes increased.

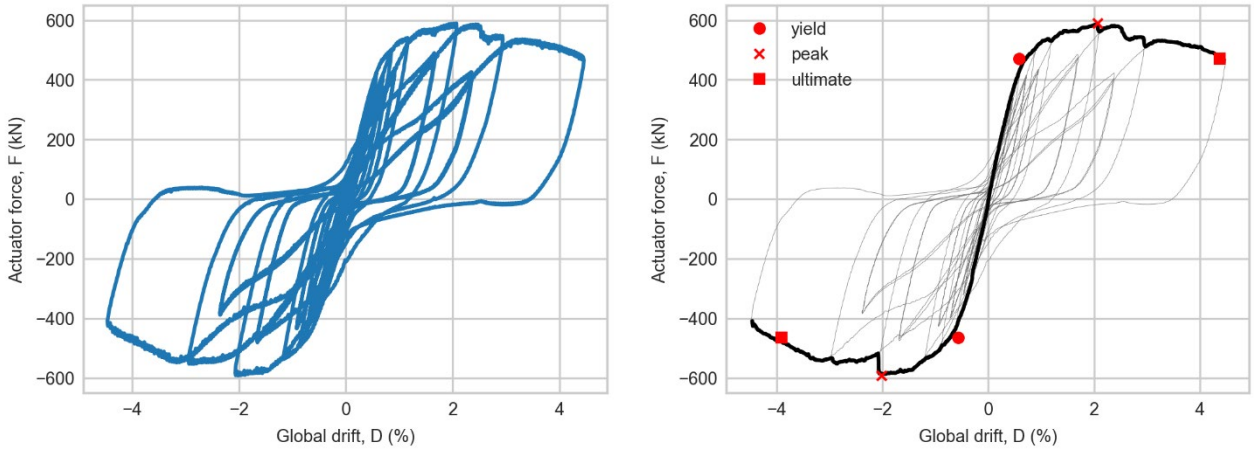

(a) (b)

Figure 22: Global drift vs. actuator force for test W41: (a) Hysteretic behaviour and (b) backbone plot with key points.

Table 7 summarizes the key results for the original specimen (W41) and the repaired specimen (W41-r). This includes the initial stiffness (K_i), yield point (D_y, F_y), peak point (D_{pk}, F_{pk}), ultimate point (D_u, F_u), and ductility (μ). The yield points were determined by the method described in the EN12512 Testing Standard [24] for load-displacement behaviour without two well-defined linear segments. The ultimate points in each loading direction were defined as the point when 20% strength loss occurred.

Table 7: Summary of results for coupled CLT wall test (W41) and re-testing of repaired specimen (W41-r).

ID	K_i (kN/mm)		F_y (kN)		F_{pk} (kN)		D_y (% drift)		D_{pk} (% drift)		D_u (% drift)		μ (D_u/D_y)	
	+	-	+	-	+	-	+	-	+	-	+	-	+	-
W41	11.9	12.1	471	-464	590	-592	0.58%	-0.56%	2.07%	-2.02%	4.37%	-3.91%	7.6	6.9
W41-r	10.7	10.2	482	-482	636	-607	0.66%	-0.69%	2.49%	-1.90%	-	-3.44%	-	5.0

The base rotation versus global base moment and base rotation versus normalized neutral axis for each pier are shown in *Figure 23a and 23b*. The plots do not include the final cycle to +/- 4.5% drift because the wall uplift exceeded the displacement capacity of several spring potentiometers and therefore the data was not adequately captured. As the coupled wall was loaded in the positive direction (i.e. actuator applying compressive force to the specimen), a greater amount of base rotation and uplift occurred in pier 2 (the tension pier), as shown in *Figure 23a*. Due to the combined moment and axial uplift force on the base of the tension pier, its HDs experienced significantly greater uplift forces and yielded more significantly than those in the compression pier.

Therefore, the rotational stiffness of the tension pier's base was reduced and it experienced a greater amount of rotation than the compression pier. An example of this is shown in *Figure 24* when the global applied moment was 3800kNm. Significant strength loss occurred in the wall pier bases, as evident in Figure a, due to yielding of the screws in the HD connections during the primary cycles, which reduced the amount of strength and stiffness in the HD connections during the subsequent cycles. The tension pier (i.e. pier 2 for positive loading or pier 1 for negative loading) frequently experienced complete uplift during the test, with no contact to the steel base plates.

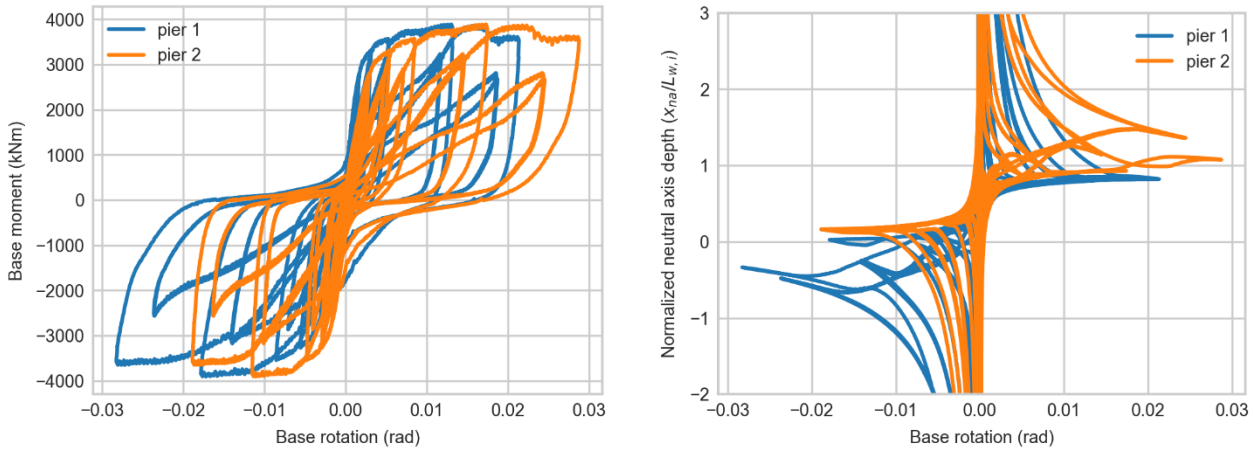

(a) (b)

Figure 23: Wall base behaviour: (a) moment vs. base rotation and (b) normalized neutral axis vs. base rotation.

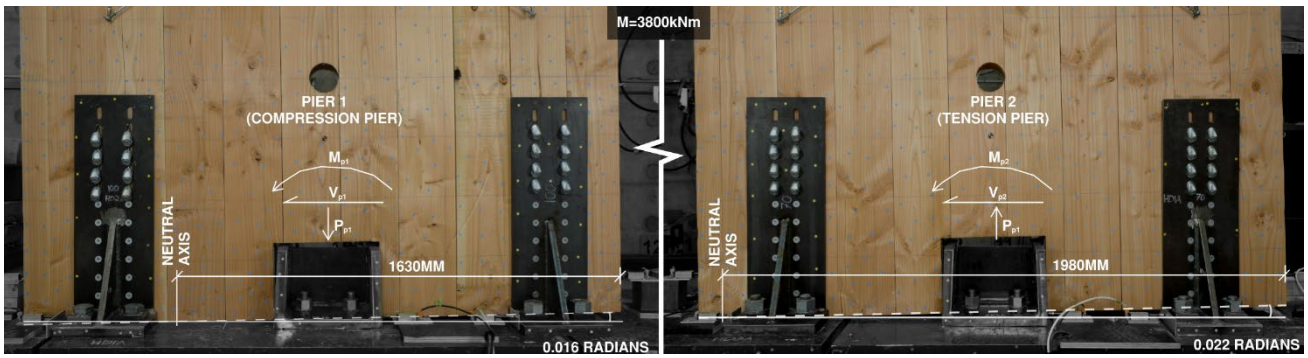

Figure 24: Base rotation and neutral axis depths of wall piers at M=3800kNm.

Table 8 includes a summary of the observed shear strains at a height of 1500mm above the wall base for the yield, peak, and ultimate points in the positive and negative directions. Regardless of loading direction, the compression pier always experienced larger shear strains because of its greater amount of contact force and related base friction force, thereby creating a stiffer lateral load path than the tension pier's base, which attracted a greater portion of the system's shear force

demand. In contrast, the tension pier was uplifted which reduced (or in some cases eliminated) its contact force with the steel bases and its engagement with the shear key, thereby reducing the amount of shear force in the tension pier. It was also observed that the shear strain magnitude of the compression pier increased from top to bottom. Therefore, the higher relative shear force in the compression pier was in part due to a transfer of shear from the tension pier to the compression pier through compressive axial forces in the beams.

Table 8: Shear strains observed in CLT wall piers at key points.

Point	Actuator displacement (mm)	Actuator force (kN)	Pier 1 shear strain at h=1500mm	Pier 2 shear strain at h=1500mm
Positive yield	35.0	403	0.00141	0.00066
Positive peak	137	590	0.00219	0.00098
Positive ultimate	288	470	0.00168	0.00101
Negative yield	-32.9	-380	-0.00048	-0.00110
Negative peak	-133	-592	-0.00054	-0.00228
Negative ultimate	-258	-465	-0.00021	-0.00185

Link beam responses

The shear force demands in the link beams were determined from the strain gauges and are plotted in *Figure 25*. The data was limited to cycles of +/-0.9% drift or less because the strain gauges de-bonded from the steel surface after a moderate level of yielding occurred. Yielding initiated in the beams at approximately 0.5% drift.

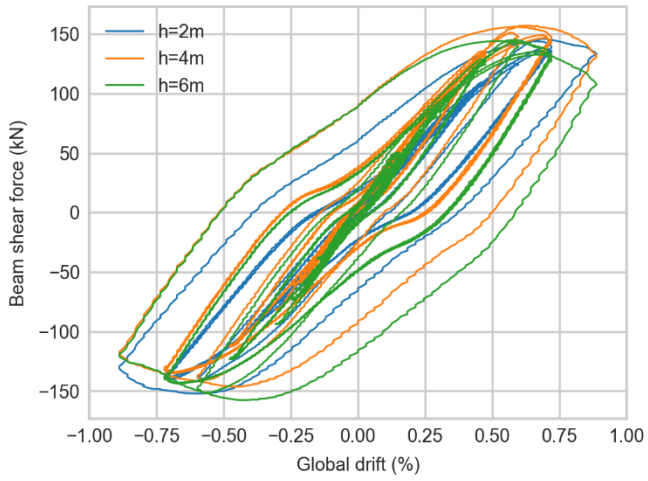

Figure 25: Link beam shear forces (Note: Data collection limited to <0.9% global drift due to strain gauge debonding after significant yielding).

The link beams experienced similar shear force magnitudes for a given drift level before yielding. This is primarily because of the relatively small height of the 2/3-scale, 3-storey wall specimen and the CLT's inherently high in-plane stiffness causing nearly uniform deformation demands on each

link beam. Taller coupled CLT walls may experience more significant in-plane deformations which would cause the shear force demands in the link beams to vary more significantly over the height of the system.

The overturning moment capacity of the coupled wall can be attributed to two components, the coupling beams and the wall bases. *Figure 26* shows the global (M) and contributing base moments calculated for the backbone response. The wall pier moments (M_1 and M_2) were calculated based on an extrapolation of the recorded curvature profile along each pier's height to determine their respective base curvatures. The base curvatures were then multiplied by the flexural stiffness of each wall using values of E=9GPa, based on the mean result of compression test data on the Douglas Fir boards, and I_{xx}=90x10^{9}mm^4 (M_i=Ø$_{base}$EI_{xx}). The base moment attributed to the link beams (M_b) was calculated using the observed shear forces multiplied by L=2.8m (where L=L_w+L_b). As discussed previously, the shear force data was not available beyond 0.9% drift, therefore, values beyond this drift level were inferred by subtracting the wall pier base moments from the global wall moment.

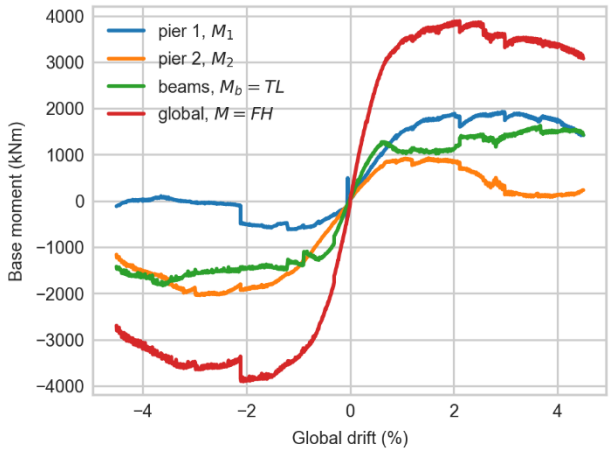

Figure 26: Distribution of base moments to the wall piers and coupling beams for the wall's backbone response.

Another form of representing the internal force distribution in the coupled wall system is with the degree of coupling factor, β. This factor is plotted in *Figure 27* for the backbone response using the observed beam shears and wall pier moments. The β factor calculated using the beam shear data is considered more reliable than the wall pier moments because the steel link beams are isotropic while the CLT piers are orthotropic and their curvatures were recorded at discrete points on the front surfaces. However, the beam shear data was limited to a maximum drift of 0.9% due to the debonding of the strain gauges and therefore both methods are shown in the plotted response. The difference between the calculated beta factors in *Figure 27* can be attributed to the more approximate nature of the β factor calculated using the pier base moments.

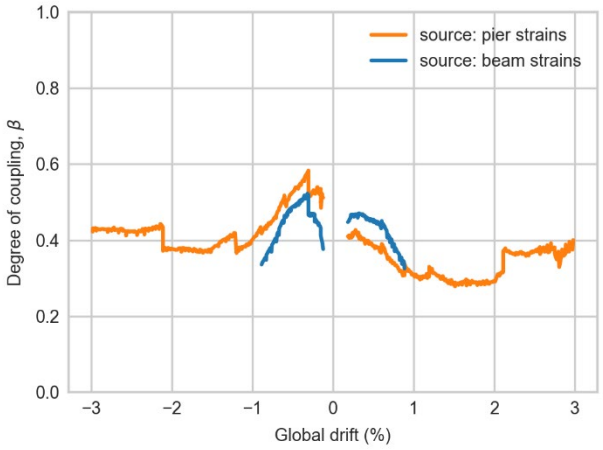

Figure 27: Degree of coupling measured by the beam strains and wall pier strains for the walls' backbone response.

The degree of coupling varied significantly as the drift level increased and the system's components yielded causing internal forces to redistribute. The factor tended to decrease until reaching a minimum value at the systems peak strength ($\beta_{F,peak,pos}$=0.31, $\beta_{F,peak,neg}$=0.38), then increased to values of 0.40 at +4.5% drift and 0.43 at -4.5% drift. Harries [10] describes a representative pushover analysis of a RC coupled wall system and also observed a reduction in β as greater levels of inelastic behaviour occurred in coupling beams and the system's internal forces redistributed. Considering the β value at the peak positive applied force, the link beams provided an additional 45% strength (calculated by 1/(1-β)) beyond what a pair of similar cantilever walls with mixed angle screw HDs would possess.

Energy dissipation

The coupled wall system exhibited a ductile failure mode and dissipated energy by yielding the steel link beams and mixed angle screw HDs. *Figure 28a* shows a bar plot of the energy dissipated in each half-cycle (cycles below 0.9% drift truncated for clarity). *Figure 28b* summarizes the equivalent viscous damping in each full cycle for the primary and first two trailing cycles of the coupled wall test.

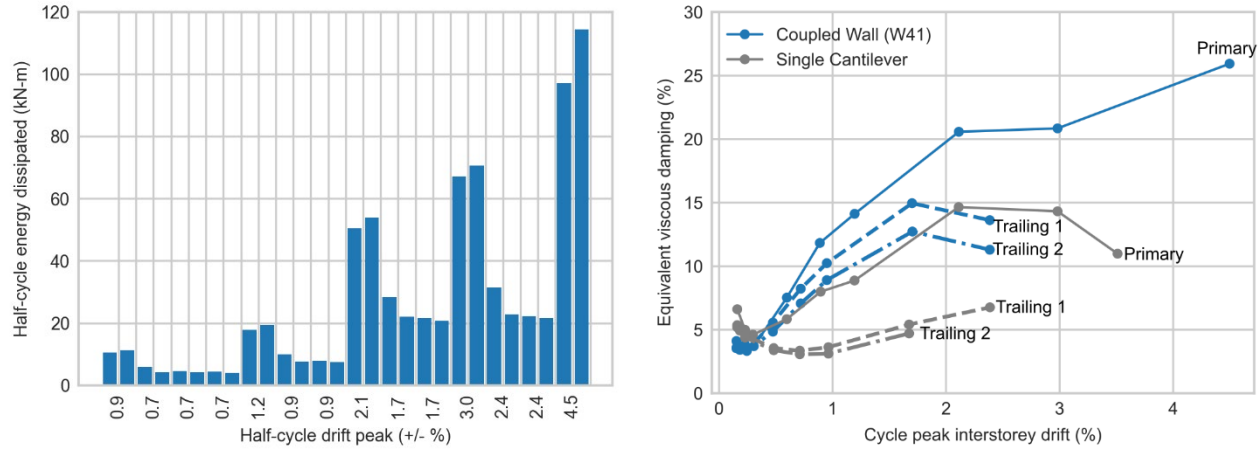

(a) (b)

Figure 28: Energy dissipation during test: (a) half-cycle energy dissipation and (b) equivalent viscous damping for full cycles.

A cantilever CLT wall with the same dimensions and base connections as the wall piers in this study was also tested using the same loading protocol. The cantilever wall test was terminated before reaching 4.5% drift, therefore, the comparison of energy dissipation is limited to +/- 3% drift (the last full cycle completed by both tests). At 3% drift, a single cantilever wall dissipated a total of 160kNm of energy, while the coupled wall in this study dissipated 480kNm. Therefore, if the coupled wall system is compared to two independent cantilever walls with the same base connections, the coupled wall system dissipated 50% more energy for the applied loading protocol to 3% drift.

The equivalent viscous damping is shown for both the coupled and single cantilever wall in *Figure 28b*. The cantilever wall did not exceed 15% in any cycle, while the coupled wall achieved more than 20% at comparable drift levels. Furthermore, the trailing cycles of the cantilever wall test exhibited approximately half of the equivalent viscous damping that was observed in its primary cycles. However, the coupled wall experienced a much smaller reduction of about one third its equivalent viscous damping when comparing the primary and trailing cycles. Furthermore, the degree of pinching in the system's hysteretic loops was significantly less in the coupled wall system. Evidently, coupled CLT wall systems dissipate a significantly greater amount of energy and experience less degradation of their energy dissipation in subsequent loading cycles than similar cantilever CLT shear walls; therefore, they are a more resilient form of LLRS.

Repair and re-testing

The tested wall was repaired to a functional state, simulating a post-earthquake recovery. Overall, the ease of reinstallation and low cost of required materials resulted in a very economic repair

method. The screws and grout of the steel link beam connections were first removed (*Figure 29a*) and the beams were lifted out from between the wall piers (*Figure 29b*). Three new beams with the same details were then installed and grout was pumped between the steel end plates and adjacent notch surfaces (*Figure 29c*). The delaminated boards at the CLT wall base toes (*Figure 30a*) were re-attached to the CLT panels with self-tapping screws (*Figure 30b* and 30c). First, Ø8x80 partially threaded washer head screws with plate washers were installed to pull the board tight to the intact CLT boards. Then a series of Ø8x260 fully threaded cylinder head screws were installed at an angle of 30 degrees to provide shear force transfer between board layers.

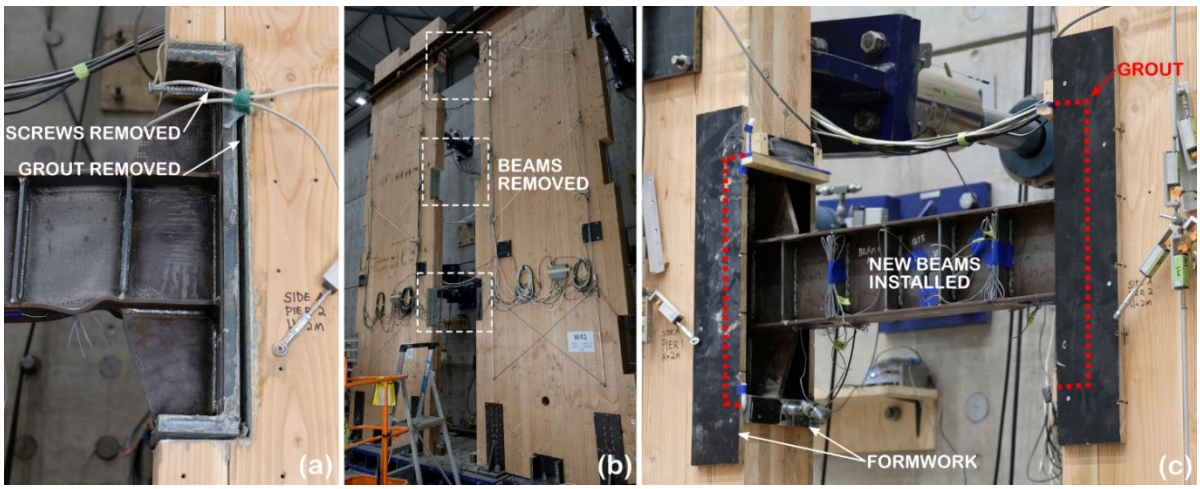

Figure 29: Repair method for damaged link beams: (a) grout and screw removal; beam removal; and (c) new beam installation.

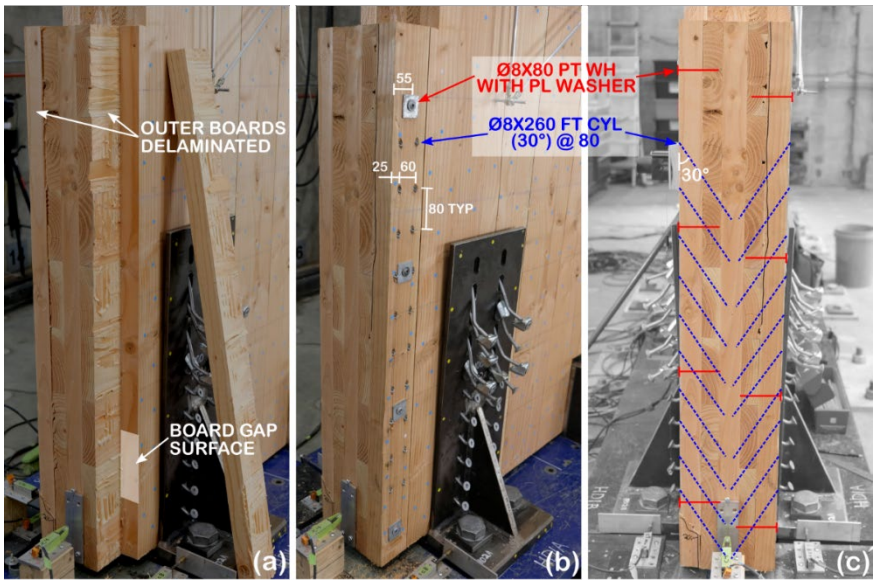

Figure 30: Repair method for delamination at CLT wall toe: (a) delaminated state, (b) isometric, and (c) elevation view of screw reinforcement.

The mixed angle screw HDs were repaired according to the methodology shown in *Figure* , following the experimental work and recommendations from Wright et al. [20]. Damage to the

specimen was concentrated at the wall's HD connections, therefore only a small region of the wall needed to be accessed for the repair. Crushing at the toes of the wall base was not severe and the authors are unaware of economical repair strategies for these regions; therefore, this was not addressed by the repair work. The repaired specimen's performance was comparable to the original wall, as shown in *Figure* and summarized in *Table* . A slightly lower initial stiffness, yield strength, and ductility ratio were observed when compared to W41, which can be partially attributed to the residual crushing at the CLT pier toes which remained from the original test. However, higher peak strength was achieved in the repaired specimen, which was mainly due to the repaired HDs being slightly stronger than the original connections, as observed in experiments by Wright et al. [20]. The small increase in peak strength (+8%) may be of some concern when retrofitting damaged coupled walls if other elements in the load path of the LLRS (e.g. diaphragm or foundation) do not possess adequate strength. The repaired specimen dissipated 827kNm, which was 5% more than the preceding test (791kN.m).

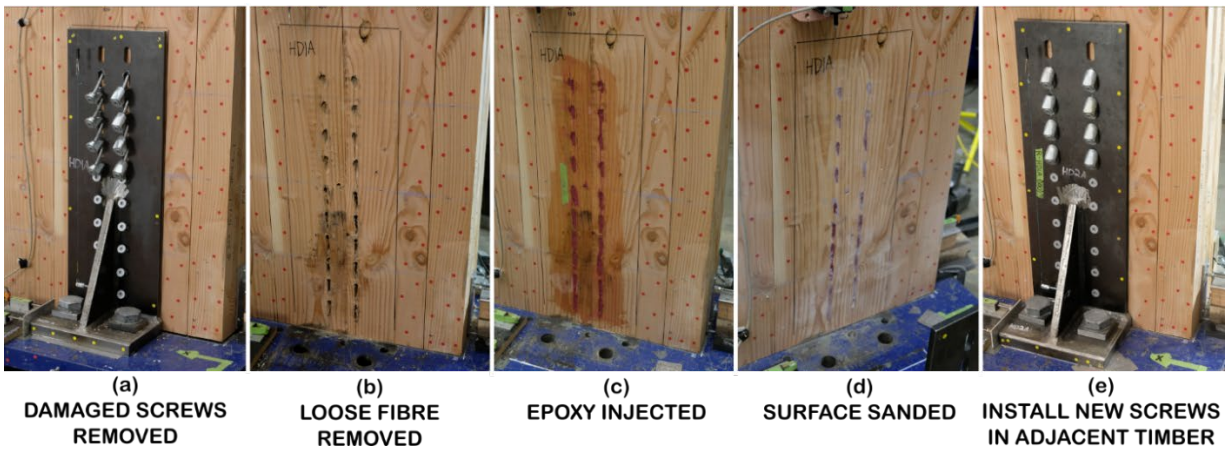

Figure 31: Repair method for mixed angle screw HD.

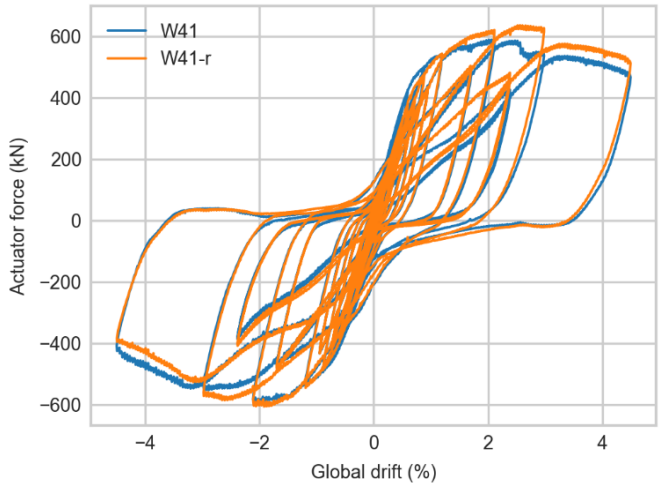

Figure 32: Comparison of original coupled wall test (W41) and repaired specimen (W41-r).

4. CONCLUSIONS

A total of seven high-capacity Douglas-fir CLT shear walls (six single wall and one coupled wall) were cyclically tested with three different aspect ratios and two types of HDs with bolts or mixed angle screws. Based on the experimental results, the following conclusions are drawn:

1. Bolted and mixed-angle screw HDs can be used to create high-capacity Douglas-fir CLT shear walls with more significant panel utilization, higher strength, and greater stiffness when compared to typical CLT walls with conventional connectors.
2. Douglas-fir CLT shear walls with bolted or mixed angle screw connections exhibit severe pinching in their hysteretic behaviour and significantly reduced equivalent viscous damping during their trailing cycles, which must be carefully considered and modelled well when creating nonlinear models or predicting peak drift responses.
3. The proposed coupled Douglas-fir CLT shear wall exhibited ductile failure mechanism through yielding of the steel link beams and mixed-angle screwed HD connections at its base, similar to the intended plastic mechanism of RC coupled walls. Therefore, the hybrid coupled CLT wall systems have the potential to be a feasible lateral load resisting system in new buildings.
4. When compared to similar cantilever CLT shear walls, the hybrid coupled wall system exhibited superior seismic behaviour as a LLRS due to its greater strength, stiffness, energy dissipation, and ductility. The degree of coupling, β, for the tested coupled CLT wall system was 0.31 and 0.38 at the peak loads in the positive and negative directions, respectively.
5. Following an earthquake event, the proposed coupled CLT wall system may be economically repaired by replacing damaged components (e.g. steel link beams and screwed HDs) if they can be reasonably accessed and the residual displacement is not significant.

Future work will use the experimental data to calibrate numerical models for analysing the system behaviour of various coupled CLT shear wall configurations subjected to earthquake loading. Additionally, the optimization of coupled CLT wall systems may be investigated by using alternative types of coupling beams, link beam-to-CLT wall connections, or base HDs.

5. REFERENCES

[1] National Building Code of Canada: 2020, (2022) v. 1, 792 p.; v. 2, 708 p. https://doi.org/10.4224/W324-HV93.

[2] American Society of Civil Engineers (ASCE), Minimum Design Loads and Associated Criteria for Buildings and Other Structures, ASCE, Reston, UNITED STATES, 2021. http://ebookcentral.proquest.com/lib/canterbury/detail.action?docID=6822239.

[3] Special design provisions for wind and seismic (SDPWS), American Wood Council (2021).

[4] S. Pei, J.W. van de Lindt, M. Popovski, J.W. Berman, J.D. Dolan, J. Ricles, R. Sause, H. Blomgren, D.R. Rammer, Cross-Laminated Timber for Seismic Regions: Progress and Challenges for Research and Implementation, J. Struct. Eng. 142 (2016). https://doi.org/10.1061/(ASCE)ST.1943-541X.0001192.

[5] M. Izzi, D. Casagrande, S. Bezzi, D. Pasca, M. Follesa, R. Tomasi, Seismic behaviour of Cross-Laminated Timber structures: A state-of-the-art review, Engineering Structures. 170 (2018) 42–52. https://doi.org/10.1016/j.engstruct.2018.05.060.

[6] European committee for Standardization (CEN), Eurocode 5. Design of timber structures - Part 1-1: General - Common rules and rules for buildings., (2003).

[7] D. Casagrande, S. Rossi, T. Sartori, R. Tomasi, Proposal of an analytical procedure and a simplified numerical model for elastic response of single-storey timber shear-walls, Construction and Building Materials. 102 (2016) 1101–1112. https://doi.org/10.1016/j.conbuildmat.2014.12.114.

[8] I. Lukacs, A. Björnfot, R. Tomasi, Strength and stiffness of cross-laminated timber (CLT) shear walls: State-of-the-art of analytical approaches, Engineering Structures. 178 (2019) 136–147. https://doi.org/10.1016/j.engstruct.2018.05.126.

[9] B. Dujic, S. Klobčar, R. Žarnić, Influence of openings on shear capacity of massive cross-laminated wooden walls, in: Coimbra, Portugal, 2006.

[10] M.P. Lauriola, C. Sandhaas, Quasi-static and pseudo-dynamic tests on XLAM walls and buildings, in: Coimbra, Portugal, 2006.

[11] M. Okabe, M. Yasumura, K. Kobayashi, T. Haramiishi, Y. Nakashima, F. Kazuhiko, Effect of vertical load under cyclic lateral load test for evaluating sugi CLT wall panel, in: Auckland, New Zealand, 2012.

[12] M. Popovski, E. Karacabeyli, Seismic Behaviour of Cross-Laminated Timber Structures, in: Lisboa, Portugal, 2012.

[13] J. Hummel, W. Seim, G. Flatscher, G. Schickhofer, CLT Wall Elements Under Cyclic Loading – Details for Anchorage and Connection, (2013) 15.

[14] G. Flatscher, K. Bratulic, G. Schickhofer, Experimental tests on cross-laminated timber joints and walls, Proceedings of the Institution of Civil Engineers - Structures and Buildings. 168 (2015) 868–877. https://doi.org/10.1680/stbu.13.00085.

[15] I. Gavric, M. Fragiacomo, A. Ceccotti, Cyclic Behavior of CLT Wall Systems: Experimental Tests and Analytical Prediction Models, J. Struct. Eng. 141 (2015) 04015034. https://doi.org/10.1061/(ASCE)ST.1943-541X.0001246.

[16] L. Pozza, R. Scotta, D. Trutalli, A. Polastri, I. Smith, Experimentally based q-factor estimation of cross-laminated timber walls, Proceedings of the Institution of Civil Engineers - Structures and Buildings. 169 (2016) 492–507. https://doi.org/10.1680/jstbu.15.00009.

[17] M. Amini, Determination of Seismic Performance Factors For Cross Laminated Timber Shear Wall System Based on FEMA P695 Methodology, PhD Thesis, Colorado State University, 2018.

[18] Z. Li, X. Wang, M. He, Experimental and Analytical Investigations into Lateral Performance of Cross-Laminated Timber (CLT) Shear Walls with Different Construction Methods, Journal of Earthquake Engineering. 26 (2022) 3724–3746. https://doi.org/10.1080/13632469.2020.1815609.

[19] M.O. Amini, J.W. van de Lindt, D. Rammer, S. Pei, Rocking Behavior of High-Aspect-Ratio Cross-Laminated Timber Shear Walls: Experimental and Numerical Investigation, J. Archit. Eng. 27 (2021) 04021013. https://doi.org/10.1061/(ASCE)AE.1943-5568.0000473.

[20] T.D.W. Wright, M. Li, D. Moroder, D. Carradine, Cyclic behaviour of hold-downs using mixed angle self-tapping screws in Douglas-fir CLT, in: Christchurch, New Zealand, 2021.

[21] L.-M. Ottenhaus, M. Li, T. Smith, Structural performance of large-scale dowelled CLT connections under monotonic and cyclic loading, Engineering Structures. 176 (2018) 41–48.

[22] New Zealand Standard, NZS 3603:1993 Timber Structures Standard, (2005).

[23] Helmut Krawinkler, Francisco Parisi, Luis Ibarra, Ashraf Ayoub, Ricardo Medina, Development of a Testing Protocol for Woodframe Structures, (2001).

[24] BSI Standards, EN 12512:2002 - Timber structures - Test methods - Cyclic testing of joints made with mechanical fasteners.

[25] G. Schickhofer, A. Ringhofer, The seimic behaviour of buildings erected in solid timber construction - Seismic design according to EN 1998 for a 5-storey reference building in CLT, (2012).

[26] New Zealand Standard, Structural Design Action, NZS1170.5: Earthquake Actions - New Zealand, (2016).

[27] American Society of Civil Engineers (ASCE), ASCE 7-22 Minimum Design Loads and Associated Criteria for Buildings and Other Structures, American Society of Civil Engineers, 2021.

[28] New Zealand Standard, NZS3404:1997 Steel structures standard (Incorporating Amendments 1 and 2), (2007).

[29] AISC, ANSI/AISC 341-16 Seismic Provisions for Structural Steel Buildings, (2016).

[30] Australia/New Zealand Standard, AS/NZS 3679.1:2016 Structural Steel - Part 1: Hot-rolled bars and sections, (2016).